"AUREL VLAICU" UNIVERSITY OF ARAD
FACULTY OF FOOD ENGINEERING, TOURISM AND ENVIRONMENTAL PROTECTION
CHEMICAL AND TECHNOLOGICAL RESEARCH CENTER

Scientific and Technical Bulletin

Series CHEMISTRY, FOOD SCIENCE & ENGINEERING

SYNTHESIS, STRUCTURAL AND PHOTOPHYSICAL PROPERTIES OF A NEW DITOPIC TERPYRIDINE-BASED PROLIGAND BEARING DISELENIDE UNITS

Adelina A. ANDELESCU, Evelyn POPA, Elisabeta-Ildyko SZERB

(Pages 46-53)

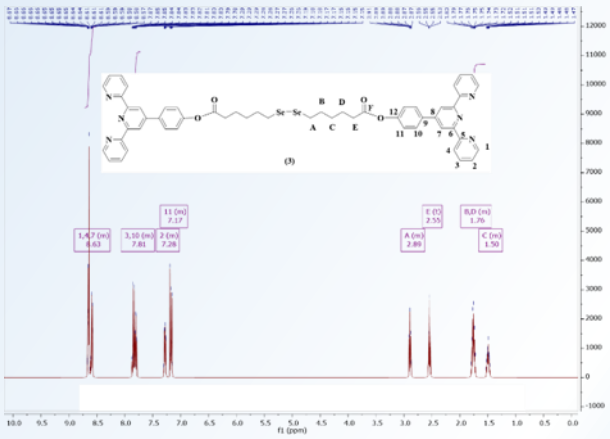

Figure A. The ^{1}H-NMR spectrum of compound 3 recorded in $CDCl_3$ and the atom labeling.

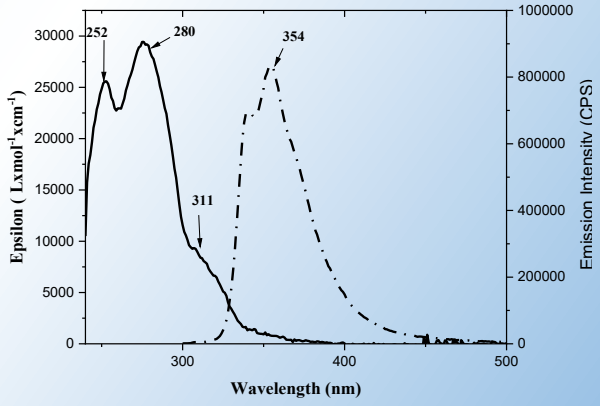

Figure B. Absorption (solid line) and emission (dashed line) of compound 3 in CH_2Cl_2 solution.

Year XXII, Vol. 21, 2024
https://www.uav.ro/jour/index.php/stb-cfse/index

“AUREL VLAICU” UNIVERSITY OF ARAD

FACULTY OF FOOD ENGINEERING, TOURISM AND ENVIRONMENTAL PROTECTION

CHEMICAL AND TECHNOLOGICAL RESEARCH CENTER

Scientific and Technical Bulletin

Series CHEMISTRY, FOOD SCIENCE & ENGINEERING

Year XXII, Vol. 21, 2024

ISSN 1582-1021

e-ISSN 2668-4764

EDITURA UNIVERSITĂȚII AUREL VLAICU ARAD

EDITURA UNIVERSITĂȚII
AUREL VLAICU
ARAD

CONTENTS

ADDRESS
Faculty of Food Engineering, Tourism and Environmental Protection,
„Aurel Vlaicu" University of Arad, Elena Dragoi St., Nr. 2, L31, Arad, Romania
Phone: 0040257369091
E-mail: dana.copolovici@uav.ro

Scientific and Technical Bulletin, Series: Chemistry, Food Science and Engineering is covered/indexed/abstracted in:

Directory of Research Journals Indexing	**Directory of Research Journals Indexing**
ROAD	**Directory of Open Access Scholarly Resources**
OCLC WorldCat	**World Cat**
Google Scholar	**Google Scholar**
CABI	**CABI**
INDEX COPERNICUS INTERNATIONAL	**Index Copernicus International**

Article

PREMISES FOR SUSTAINABLE ENTREPRENEURIAL DEVELOPMENT OF EASTERN PARTNER COUNTRIES

Radu-Lucian BLAGA[1,2], Florin-Lucian ISAC[1], Vanina-Adoriana TRIFAN[1,3], Oana BRÎNZAN[4], Eugenia ȚIGAN[4], Simona GAVRILAȘ[4,*]

[1]Faculty of Economics, "Aurel Vlaicu" University of Arad, 10 Paul Chinezul Str., Arad, Romania
[2]Center for Research in Sustainable Bio-Eco-Economy, "Aurel Vlaicu" University of Arad, 77 Revoluției Bd., Arad, Romania
[3]Center for Applied Ethics Studies, "Aurel Vlaicu" University of Arad, 10 Paul Chinezul Str., Arad, Romania
[4]Faculty of Food Engineering, Tourism and Environmental Protection," Aurel Vlaicu" University of Arad, 2-4 Elena Drăgoi Str., 310330 Arad, Romania;
Corresponding author email: simona.gavrilas@uav.ro

Abstract: *Culture and entrepreneurship are complex and interrelated social concepts. The paper aims to determine the importance of national culture for entrepreneurship progress in the Eastern Partnership (EaP) region. The article focuses on a meta-analysis of the inputs integrated into a European Union Policy Index. It aimed to underline the nature of specific interrelation mechanisms of the cultural dimensions that could contribute to developing a performant entrepreneurial environment. The correlation analysis used in the paper detects the most "sensitive" pairs of variables related to national culture and entrepreneurship activities. Results show a highly significant relationship between the Motivation Towards Achievement and Success index and a large part of the dimensions of the sustainable entrepreneurial development of EaP countries, especially Internationalization and Support Services for Small and Medium Enterprises SMEs and start-ups. Another significant relationship is between Individualism and the Development of Entrepreneurial Activities in the analyzed countries.*

Keywords: cultural dimensions, business progress, advancement of enterprising activities, Eastern Partnership countries, correlation analysis, economic well-being.

INTRODUCTION

In its general acceptance as an attitudinal and productive factor, entrepreneurship is widely believed to contribute to the economic development and prosperity of communities, regions, and countries (Ordeñana et al., 2020). As Anderson et al. stated (Anderson, 2000), entrepreneurship and entrepreneurial performance are a product of the businessperson and the context, the social and economic circumstances in which they perform.

Public policies pursue ambitious initiatives to help SMEs (small- and medium-sized firms) innovate and create jobs, benefit from digitalization, and become global leaders in sustainable practices (Ahadi and Kasraie, 2020, Gaweł and Mińska-Struzik, 2023, Jha et al., 2018, Nica, 2021).

The European Union (EU) regards successful entrepreneurial activity as strategically essential for economic well-being. Therefore, the EU aims to streamline SMEs entrepreneurship. EU and six neighboring countries, Armenia, Azerbaijan, Belarus, Georgia, the Republic of Moldova, and Ukraine, created the Eastern Partnership (EaP), a joint initiative that aims to help the economies of these countries become more inclusive and resilient to shocks.

Sustainable entrepreneurship, which successfully merges traditional business objectives with environmental and social considerations, is becoming increasingly significant globally. In the specific context of Eastern Partnership (EaP) countries, fostering sustainable entrepreneurship presents a variety of noteworthy benefits that are integral to economic and social development.

Promoting sustainable entrepreneurship can be crucial in effectively addressing pressing environmental challenges. Encouraging businesses to adopt eco-friendly practices creates opportunities for innovation and the development of new markets, ultimately

yielding significant economic benefits. This dual focus helps mitigate environmental degradation and supports sustainable economic opportunities for local communities.

A strong emphasis on sustainable practices can improve resource efficiency and enhance small and medium-sized enterprises (SMEs) competitiveness. By optimizing their use of resources and implementing sustainable business models, these enterprises can reduce operational costs, thereby improving their overall financial performance in a competitive marketplace.

A proper alignment with European Union sustainability standards can serve as a critical stepping stone for EaP countries, potentially easing the pathway to future integration with the EU. By adopting these standards, businesses in the region enhance their credibility and demonstrate a commitment to sustainability, which can positively influence trade relations and investment opportunities.

Promoting sustainable entrepreneurship will likely attract impact investors and increase access to green finance. As the demand for socially and environmentally responsible investment grows, firms prioritizing sustainability may find it easier to secure funding, allowing further growth and innovation.

So, future research should delve into the influence of cultural factors on adopting sustainable entrepreneurship practices in the EaP region. Understanding these dynamics will be essential for tailoring approaches encouraging widespread acceptance and implementation of sustainable business models, ultimately contributing to the region's long-term economic and environmental resilience.

The literature review in the field determined us to settle the paper's aims. The first one seeks to *evaluate the importance of national culture for sustainable entrepreneurship development in the Eastern Partnership region*, organized around the SBA (*Small Business Act*) principles.

The second objective was to *settle the importance of national culture for entrepreneurship durable expansion* in the Eastern Partnership region, organized around the SBA principles. The SBA assessment is a key tool for improving the businesses in EaP countries and strengthening institutions and good governance (OECD et al., 2020).

Considering the data from the literature analysis, we hypothesize that *certain dimensions of national culture* influence *particular dimensions of entrepreneurial expansion* in Eastern Partnership countries. Hence, we formulated the following assumptions, which underwent testing in the paper:

H1: *The cultural dimension of Hofstede's model, known as Motivation Towards Achievement and Success (formerly the dimension of masculinity), impacts The Advancement of Entrepreneurial Activity*.

H2: *As a cultural dimension in Hofstede's model, Individualism impacts The Advancement of Entrepreneurial Activity*.

The Hofsted's specific elements in this study are derived from analyzing the national cultural background. The aim was to understand influential behaviors and values better. Such aspects provide a useful framework for understanding cultural differences and facilitating intercultural interactions, especially in business.

MATERIALS AND METHODS

Method

This study analyzed the results of applying Hofstede's cultural dimensions model statistically. The method consists of a theoretical framework developed by researcher Geert Hofstede that helps understand cultural differences between nations and groups. Hofstede conducted extensive research in several countries, analyzing human behaviors in the context of cultural diversity. The pattern is based on the identification of six cultural dimensions, which are characteristics that describe fundamental differences between national cultures. It can be used to better understand the dynamics of international interactions, as in business media, and to explain behavioral divergences between individuals or groups from different cultures.

Materials

The statistics evaluated were integrated into the SME Policy Index: Eastern Partner Countries

material in 2020. The Hofstede (six) data express culturally motivated attitudes and social reaction patterns, which can be attributed to country inhabitants or territories. Our data, Hofstede's six cultural dimension matrix (HOF-6) is of 6 x 6 size, reflecting the countries Armenia, Azerbaijan, Belarus, Georgia, the Republic of Moldova, and Ukraine, and the equivalent Hofstede scale, Table 1. The Hofstede data was chosen because it covers a longer period and exists for most European countries.

Table 1 Cultural dimensions according to Hofstede

Cultural dimensions	Abbrev.	Operational definitions
Power distance	POW	The degree to which the less powerful in society expect and accept unequal power distribution.
Individualism/Collectivism	IND	Individualized responsibility and problem-solving vs. more collective variants. The former leans towards egoism, while the latter borders on unconditional group loyalty.
Motivation towards achievement and success (Masculinity/Femininity)	MAS	A high score (Decisive) on this dimension indicates that society will be driven by competition, achievement, and success, with success being defined by the winner / best in the field. A Consensus-oriented society is one where quality of life is the sign of success, and standing out from the crowd is not admirable.
Uncertainty Avoidance	UNC	Expresses a degree of risk aversion.
Long Time vs. Short Time Orientation	LTO	LTO values future payoffs, planning, and patience; STO values fast payoffs, possibly in response to social uncertainty or instability.
Indulgence vs. Restraint	IDL	Indulgence allows for the gratification of basic, natural human drives of, i.e., enjoying life and having fun." Restraint" applies strict social norms instead.

Note: All values are within [0-100]. Abbreviations introduced in column two are used later in our data analysis.

Source: interpreted after https://www.hofstede-insights.com/country-comparison-tool

The other data matrix we confront is the 6 x 12-twelve SME Policy Index for EaP dimensions matrix (SME EaP-12), which has analog complex entrepreneurial activity indicators described in Table 2.

Table 2 The detailed SME assessment framework and its links to the Small Business Act Principles-Statistical dimensions for assessment of sustained expansion

SBA principle	Abbrev.	SME Policy Index dimension	Related sub-dimensions
1. Create an environment in which entrepreneurs and family businesses can thrive and entrepreneurship is rewarded.	ENT	Entrepreneurial learning and women's entrepreneurship	Entrepreneurial learning; Women's entrepreneurship
2. Ensure that honest entrepreneurs who have faced Bankruptcy quickly get a second chance.	SEC	Bankruptcy and Second Chance for SMEs	Preventive measures; Survival and bankruptcy procedures; Promoting second chance
3. Design rules according to the "think small first" principle.	TSF	Institutional and regulatory framework for SME policy	Institutional framework; Legislative and regulatory simplification and application; Public-private consultations (PPCs)
4. Make public administration responsive to SMEs.	RES	Operational environment for SMEs	E-government services; Business licences and permits; Company registration; Tax compliance procedures for SMEs
5 Adapt public policy tools to SME needs.	PPN a.	Support services for SMEs and start-ups	SME support services provided by the government; Government initiatives stimulating private business development services
	PPN b.	Public procurement	Public procurement
6. Facilitate SME access to finance and develop a legal framework and business	FIN	Access to finance for SMEs	Legal and regulatory framework; Bank financing; Non-bank financing;

environment supportive of timely payments in commercial transactions.			Venture capital; Financial literacy
7. Help SMEs benefit more from the opportunities the Single Market offers.	SIMA	Standards and technical regulations	Overall coordination and general measures to adopt EU product standards and regulations; Approximation with the EU Acquis; SMEs Access to Standardisation
8. Promote the upgrading of skills and all forms of innovation.	INNO a.	SMEs skills	SMEs skills
	INNO b.	Innovation	Policy framework for innovation; Government support services for innovative SMEs; Government financial support for innovative SMEs; Non-technological innovation and diffusion of innovation
9. Enable SMEs to turn environmental challenges into opportunities.	ENV	SMEs in a green economy	Environmental Policies; Incentives and instruments for greening SMEs operations
10. Encourage and support SMEs to benefit from growth markets.	INT	Internationalisation of SMEs	Export promotion; Integration of SMEs into global value chains; OECD Trade Facilitation Indicators; SME use of e-commerce

Note: Abbreviations from column two are the short names used later in our data analysis, and column Source: (OECD et al., 2020).

The independent variable of *national culture* was selected due to its constant evolution. The conceptual content of these dimensions was derived from Hofstede's works and those of his collaborators (Hofstede et al., 2012, Hofstede et al., 2004). The values for these dimensions were obtained from https://www.hofstede-insights.com/fi/product/compare-countries. The numerical values of this variable were converted into categorical variables based on Sturges H's model for all six cultural dimensions.

The dependent variable, generically called *The Advancement of Entrepreneurial Activity* of EaP countries, is represented by the SME Policy Index for EaP, the unique multi-criteria benchmarking tool, representing a key tool for the progress of the business environment and SMEs in the EaP region. It is calculated based on SBA principles and contains dependent random variables because they do not satisfy a mathematical property of probabilistic independence. The indicator's calculation method and data collection are set by SME Policy Index (OECD et al., 2020). These variables are categorical and obtained through qualitative analysis using indicators and methods starting from applying questionnaires, focus groups, and statistical analysis data (Agresti, 2012, Ataei et al., 2020).

The current study's objectives were met by applying multivariate analysis to ascertain correlations of two categorical data sets, following the Spearman and Kendal techniques as non-parametric alternatives to Pearson's correlation. The reduction of detailed measurements into ordinal numbers enabled the evaluation of complex data based on specific criteria. Analysis of ranked (categorical) data typically mandates the employment of non-parametric statistics (Tofallis et al., 2022). They allow the identification of simultaneous correlation relations between two or even more matrices (Chen et al., 2021) with different features (columns).

The research approach initially considered was designed based on the four possible situations: *a strong direct possible association between the data*, an *indirect link between them*, *none possible*, or *one of uncertainty that needed a deeper consideration at the level of subsidiary components*. Spearman and Kendal's correlations follow curvilinear, monotonic relationships for ordinal (categorical) data.

RESULTS AND DISCUSSIONS

From the Spearman and Kendal correlation analysis, for Hofstede's six cultural dimensions and the twelve dimensions of the advancement of entrepreneurial activity, through the SME

Policy Index for Eastern Partner Countries (EaP), it emerges that certain cultural dimensions evolve in the same sense and direction as dimensions of entrepreneurial progress so that only an absence of correlation was identified, that between *Power distance* (1) and each dimension of entrepreneurial progress. The most "*sensitive*" pairs of variables related to the culture and entrepreneurial activity advance of EaP countries can be seen in Tables 3 and 4.

Table 3 Most influential seven absolute correlations from HOF-6 vs. SME EaP-12 for Correlation Analysis (CA)

No.	Hofstede-6 dimension	SME Policy Index for EaP-12 dimension	p-value	Linear correlation coefficients from CA[1]
1	Motivation Towards Achievement And Success/ Masculinity (3)	Internationalization-INT (9)	*0.02*	+0.878
2	Individualism (2)	Institutional and regulatory framework for SME policy-TSF (1)	*0.04*	-0.828
3		Internationalization-INT (9)	*0.04*	-0.828
4		Support services for SMEs and start-ups (Business development services-BDS)-PPNa. (10)	*0.04*	-0.828
5	Motivation Towards Achievement And Success/Masculinity (3)	Support services for SMEs and start-ups (Business development services-BDS)-PPNa. (10)	0.13	+0.683
6	Long term orientation (5)	Access to finance for SMEs-FIN (6)	0.25	-0.555
7	Long term orientation (5)	Support services for SMEs and start-ups (Business development services-BDS)-PPNa. (10)	0.25	-0.555

Source: Author's computation.

Table 4 Most influential seven absolute correlations from HOF-6 vs. SME EaP-12 for Correlation Analysis (CA)

No.	Hofstede - 6 dimension	SME Policy Index for EaP-12 dimension	p-value	Linear correlation coefficients from CA[2]
1	Motivation Towards Achievement And Success/ Masculinity (3)	Internationalization-INT (9)	0.05	+0.775
2	Individualism (2)	Institutional and regulatory framework for SME policy-TSF (1)	0.06	-0.730
3		Internationalization-INT (9)	0.06	-0.730
4		Support services for SMEs and start-ups (Business development services-BDS)-PPNa. (10)	0.06	-0.730
5	Motivation Towards Achievement And Success/ Masculinity (3)	Support services for SMEs and start-ups (Business development services-BDS)-PPNa. (10)	0.13	+0.602
6		Institutional and regulatory framework for SME policy-TSF (1)	0.28	+0.430
7		SMEs in a green economy (Green economy)-ENV (12)	0.28	-0.430

Source: Author's computation.

The cultural dimension identified by Hofstede, *Motivation Towards Achievement and Success/Masculinity*, is the most sensitive to the entrepreneurial activities improvement at the level of the EaP countries. From the data analysis, we can say that this cultural dimension positively influences a large part of the dimensions of the entrepreneurial activities durable expansion in the analyzed countries: *The Institutional and Regulatory Framework for SME Policy Development*, *The Business Environment*, *The Competencies of SMEs*, Access to finance, *Public Procurement*, *Internationalisation*, *Business Development Services*, *Innovation Policy*. But, at the same time, it negatively impacts other dimensions of entrepreneurial failures, such as *Bankruptcy and Second Chance*, *Standards and Regulations*, and the *Green Economy*. It is relatively statistically significant, with values close to p-values equal to 0.05, Tables 3 and 4.

[1] Correlation coefficients according to Spearman

[2] Correlation coefficients according to Kendall

The more the EaP countries have a larger number of potential entrepreneurs characterized by a more pronounced masculinity, the higher they will succeed in penetrating the international market (Shneor et al., 2017), while at the same time increasing the profitability of internationalized firms (Gaganis et al., 2019). The Eastern Partnership countries are less oriented towards achievement and success (in particular: Belarus, Ukraine, and Moldova), less competitive and sensitive to material rewards or financial efficiency, and therefore less concerned with developing international partnership relations.

Adapting public policy instruments to the needs of SMEs through Business Development Services (BDS) is an element of progress in entrepreneurial activities that is sensitive in the context of our research. In the case of most EaP countries, with a low *Motivation Towards Achievement and Success/Masculinity*, adapting public policies to the needs of the business environment has no chance of developing positively in the given cultural context. Public institutions are mainly incentives for economic activity, but in societies where the masculinity index is reduced, they discourage entrepreneurship; people are less ambitious and daring and do not support the action with current measures. On the other hand, the entrepreneurship approach is less in societies oriented toward the cultural dimension of femininity (Çelikkol et al., 2019, Huggins and Thompson, 2012).

The relationship *between Motivation Towards Achievement and Success/Masculinity* and SMEs in a green economy (*Green Economy*) explains the relationship in the opposite direction. Countries with a cultural orientation towards feminism (such as Belarus, Moldova, and Ucraina) are more oriented towards unpolluted resources and prefer supporting SMEs to turn environmental challenges into opportunities (Pelau and Pop, 2018). This cultural trait may predispose these societies to more readily embrace sustainable business practices and green policies. Thus, environmental policies, incentives, and operational tools for greening SMEs can be better considered in these countries. The *Green Economy* dimension assesses how well countries support SMEs adopting sustainable practices and technologies. Such vision includes policies promoting energy efficiency, adopting renewable energy, reducing waste, and eco-innovation among small businesses. Improving performance in this area is crucial for long-term economic resilience and environmental sustainability in the EaP region.

In conclusion, the *Motivation Towards Achievement and Success*, as a cultural dimension of Hofstede's model, influences the advancement of entrepreneurial activity, especially about the dimensions of *Internationalization and Support Services for SMEs and start-ups* (*Business Development Services*), thus confirming the study's first hypothesis.

Considering the results obtained it would be advisable to create an enabling environment that encourages motivation to achieve and succeed, to stimulate the progress of entrepreneurial activity in terms of internationalization and development of SMEs and start-ups. Such a goal could be obtained by combining financial, educational, and technological support, developing international partnerships and an environment in which risks are strategically managed. Thus, entrepreneurs will be motivated to build successful businesses and expand them into global markets.

The cultural dimension of *Individualism* identified by Hofstede is sensitive to the forward movement of entrepreneurial activities at the level of the EaP countries. It is relatively statistically significant, with values close to p-values of 0.05, as shown in Tables 3 and 4. It interacts in the opposite direction with each dimension of entrepreneurial progress, except for certain dimensions, namely *Bankruptcy and Second Chances,* and *Green Economy*. *Individualism* does not negatively affect these dimensions of entrepreneurial feasible evolution, i.e., they move in the same direction.

When analyzing the correlation between the cultural dimension of *Individualism* and the dimension of the *Institutional and Regulatory Framework for the Development of SME Policies*, a statistically significant high-confidence correlation is

observed, which shows that the increase of the first causes the second decrease.

The dimensions of entrepreneurial progression strongly negatively affected by the growth of *Individualism* are *Internationalisation and Business Development Services*. The Spearman correlation shows that the more the cultural dimension of *Individualism* increases, the more the dimension of entrepreneurial advancement *Internationalisation* decreases. The data have a highly reliable and statistically significant correlation. All these aspects related to *Individualism* confirm the second hypothesis from which the research started.

Accepting the last assumption could give policymakers the direction for encouraging and supporting an entrepreneurial culture that promotes personal autonomy, individual initiative, and responsibility. In societies with a strong emphasis on individualism, entrepreneurs are often motivated by the desire to build their businesses and pursue their dreams. In such conditions it is essential to support personal initiative and the desire for individual success, but also to provide concrete support through policies and instruments that support entrepreneurial autonomy, encourage personal responsibility, and facilitate access to strategic resources. Ensuring such conditions will motivate entrepreneurs to follow their vision and build sustainable and innovative businesses.

Given all these research results, it is considered appropriate to mention that the opposite of *Individualism* is *Collectivism* and that all the countries analyzed have a specific common collectivist history. The results of the research carried out are, to some extent, confirmed by the literature in this area. Some authors (Autio et al., 2013, Wennberg et al., 2013) propose that *Collectivism* can be detrimental to business entry, but it promotes business growth in the case of emerging economies. Pinillos and Reyes show that a collectivist culture tends to increase entrepreneurial behavior in countries with emerging economies (Pinillos and Reyes, 2011). At the level of individual firms, a stronger association between innovation and growth can be observed in collectivist cultures (Cacciotti and Hayton, 2017).

The countries considered in this study are in a period of transition and development, and their economic, educational, and technological development situation varies significantly. High-tech integration is an area of rapid growth, but there are still large disparities between countries. While Ukraine and Armenia have made significant progress in IT and education, Moldova and Belarus face greater challenges. Azerbaijan and Georgia are on track to rapidly diversify and modernize their technology sectors.

CONCLUSIONS, LIMITATIONS AND FUTURE PERSPECTIVES

The first limitation of the study is the consideration of the relationship between culture and entrepreneurial performance of the emerging countries analyzed without including data sets covering complementary variables such as GDP, education levels, and technology adoption. This holistic approach could represent the starting point for a new research perspective. Another constraint of this research was the limited data available on the countries of EaP paternity.

Results may also be checked against adding cultural dimensions other than Hofstede's. The statistical analysis highlights certain common aspects of the six EaP countries, taken into research, namely that certain cultural traits statistically significantly impact certain entrepreneurial dimensions. Of course, on a broader look, these cultural dimensions probably do not represent a characteristic of this country in particular. They are elements that generally affect certain aspects of durable entrepreneurial improvement. The specificity of the research is that it highlighted that these influences are statistically significant.

As *improving market access* and *internationalization* represented the weak bridges in the past, gradually improved from the analysis of the evolution of entrepreneurial advances in these countries, can be seen. Still, the current research shows us some levers contributing to this breaking and certain cultural dimensions.

In the case of *Individualism*, it is not considered a bad or good dimension but only an

excess of a certain social/cultural trait dimension that can boost or even inhibit the development of entrepreneurship in a certain direction. For this reason, it is considered that observing these aspects, they can be rebalanced by civil societies in the six EaP countries. It is believed that for entrepreneurial progress in EaP countries, a vital factor is the education of young people, continuous training in the field, and the promotion of good practices inspired by the experience of other cultures.

Integrating sustainability principles will be crucial as EaP countries continue to develop their entrepreneurial ecosystems. Policymakers should consider how cultural factors might influence adopting sustainable practices and tailor their approaches accordingly.

Given Hofstede's aim to contribute to understanding cultural differences between nations, the present study considered countries with great aesthetic, religious, and political diversity. However, they share a common history, with geopolitical conflicts of recent decades, which makes the region dynamic and complex in terms of international relations.

Religious differences profoundly influence relationships among Eastern Partnership countries, often intertwining with existing political and social divides. A salient example can be observed in Georgia, where the Orthodox Church exerts significant influence over both the political and cultural landscape. This institution has actively opposed European Union-supported anti-discrimination initiatives, thereby generating tensions that complicate Georgian aspirations for EU integration and alignment with Western democratic values (Rahimov, 2024).

Similarly, in Ukraine, the government has strategically utilized the establishment of an independent Orthodox Church, enhancing the societal sway of religious institutions while simultaneously fostering a climate of increased intolerance toward religious minorities (United, 2023). The resurgence of religious identity in the post-Soviet context further complicates the inter-country relationships within the region. Most of the population in various Eastern Partnership countries now identifies with a religion, predominantly Orthodox Christianity or Roman Catholicism.

This revival of religious affiliation has contributed to more conservative social attitudes, particularly among younger generations in Central and Eastern Europe. These individuals exhibit lower levels of acceptance towards Muslims, Jews, same-sex marriage, and legal abortion compared to their peers in Western Europe. The resulting religiously-based social perspectives can significantly hinder regional cooperation and alignment with European Union values, thereby straining relationships between more progressive and conservative EaP nations.

Recent internal conflicts and external influences can rapidly alter cultural and social dynamics. Hofstede's dimensions are built on general trends but do not consider in detail how national identities evolve in different contexts, where regions and ethnic groups may have very different visions. Its research bases consisted of a relatively small sample, relying mainly on employees of an international organization. Based on this consideration, it could be said that his results apply primarily to the business environment and may not fully reflect the cultural variability of the entire population of a country. When religious and national traditions play a significant role in daily life, applying Hofstede's dimensions may ignore important aspects of social or political behavior.

A study of Hofstede's cultural dimensions applied to the countries mentioned in this study can provide a general view of cultural differences but must be used cautiously. It is essential to consider each country's political, historical, geographical, and religious context and recent developments that may significantly influence learned values and attitudes.

Future research will consider the expansion of the investigation context on other influencing factors on entrepreneurship, such as well-being, GDP, the level of education, degree of digitization and computerization, etc., but also on some comparative analyses with other European countries. Another future direction of research could be one oriented toward the role of organizational culture in shaping entrepreneurial orientations.

Using Hofstede's dimensions can be useful for understanding differences and similarities between cultures, especially if the study is conducted with an updated framework that considers current socio-economic and political realities. These could provide important insights for managing diversity in business environments, in education, and in the context of international relations, but must be conducted with attention to the complexity and rapid changes in different regions of the world.

REFERENCES

AGRESTI, A. 2012. *An Introduction to Categorical Data Analysis,* Hoboken, New Jersey, John Wiley & Sons, Inc. https://mregresion.wordpress.com/wp-content/uploads/2012/08/agresti-introduction-to-categorical-data.pdf

AHADI, S. & KASRAIE, S. 2020. Contextual factors of entrepreneurship intention in manufacturing SMEs: the case study of Iran. *Journal of Small Business Enterprise Development,* 27**,** 633-657. https://doi.org/10.1108/JSBED-02-2019-0074

ANDERSON, A. R. 2000. The protean entrepreneur: the entrepreneurial process as fitting self and circumstance. *Journal of Enterprising Culture,* 8**,** 201-234. http://dx.doi.org/10.1142/S0218495800000127

ATAEI, Y., MAHMOUDI, A., FEYLIZADEH, M. R. & LI, D.-F. 2020. Ordinal priority approach (OPA) in multiple attribute decision-making. *Applied Soft Computing,* 86**,** 105893. https://doi.org/10.1016/j.asoc.2019.105893

AUTIO, E., PATHAK, S. & WENNBERG, K. 2013. Consequences of cultural practices for entrepreneurial behaviors. *Journal of International Business Studies,* 44**,** 334-362. https://doi.org/10.1057/jibs.2013.15

CACCIOTTI, G. & HAYTON, J. C. 2017. National culture and entrepreneurship. *The Wiley handbook of entrepreneurship***,** 401-422. https://doi.org/10.1002/9781118970812.ch18

ÇELIKKOL, M., KITAPÇI, H. & DÖVEN, G. J. 2019. Culture's impact on entrepreneurship and interaction effect of economic development level: An 81 country study. *Journal of Business Economics Management,* 20**,** 777-797. https://doi.org/10.3846/jbem.2019.10180

CHEN, Y.-L., KOLAR, M. & TSAY, R. S. 2021. Tensor canonical correlation analysis with convergence and statistical guarantees. *Journal of Computational Graphical Statistics,* 30**,** 728-744. https://doi.org/10.1080/10618600.2020.1856118

GAGANIS, C., PASIOURAS, F. & VOULGARI, F. 2019. Culture, business environment and SMEs' profitability: Evidence from European Countries. *Economic Modelling,* 78**,** 275-292. https://doi.org/10.1016/j.econmod.2018.09.023

GAWEŁ, A. & MIŃSKA-STRUZIK, E. 2023. The digitalisation as gender equaliser? The import and export of digitally delivered services in shaping female entrepreneurship in European countries. *International Journal of Gender Entrepreneurship*. https://doi.org/10.1108/IJGE-08-2022-0141

HOFSTEDE, G., HOFSTEDE, G. & MINKOV, M. 2012. *Culturi și organizații. Softul mental. Cooperarea interculturală și importanța ei pentru supraviețuire,* Bucharest, Romania, Humanitas, for Romanian version. https://humanitas.ro/assets/media/culturi-si-organizatii.pdf

HOFSTEDE, G., NOORDERHAVEN, N., THURIK, R., UHLANER, L. M., WENNEKERS, A. R. & WILDEMAN, R. E. 2004. Culture's role in entrepreneurship: self-employment out of dissatisfaction. *In:* TERRENCE E. BROWN, J. U. (ed.) *Innovation, Entrepreneurship and Culture.* Elgaronline. https://doi.org/10.4337/9781845420550.00014

HUGGINS, R. & THOMPSON, P. 2012. Entrepreneurship and community culture: A place-based study of their interdependency. *Entrepreneurship Research Journal,* 2**,** 000010220221575665 1045. https://doi.org/10.2202/2157-5665.1045

JHA, P., MAKKAD, M. & MITTAL, S. 2018. Performance-oriented factors for women entrepreneurs–a scale development perspective. *Journal of Entrepreneurship in Emerging Economies,* 10**,** 329-360. https://doi.org/10.1108/MD-03-2022-0305

NICA, M. 2021. Economic development and business creation. *Economic Change Restructuring,* 54**,** 219-239. https://doi.org/10.1007/s10644-020-09274-9

OECD, UNION, E., FOUNDATION, E. T. & DEVELOPMENT, E. B. F. R. A. 2020. *SME Policy Index: Eastern Partner Countries 2020*. https://www.oecd-ilibrary.org/content/publication/8b45614b-en

ORDEÑANA, X., VERA-GILCES, P., ZAMBRANO-VERA, J. & AMAYA, A. 2020. Does all entrepreneurship matter? The contribution of entrepreneurial activity to economic growth. *Academia Revista Latinoamericana de Administración,* 33**,** 25-48. https://doi.org/10.1108/ARLA-11-2018-0256

PELAU, C. & POP, N. A. 2018. Implications for the energy policy derived from the relation between the

cultural dimensions of Hofstede's model and the consumption of renewable energies. *Energy Policy,* 118**,** 160-168. https://doi.org/10.1016/j.enpol.2018.03.042

PINILLOS, M.-J. & REYES, L. 2011. Relationship between individualist–collectivist culture and entrepreneurial activity: evidence from Global Entrepreneurship Monitor data. *Small Business Economics,* 37**,** 23-37. https://doi.org/10.1007/s11187-009-9230-6

RAHIMOV, R. 2024. *Georgia's Civilizational Dilemma: For or Against Europe?* [Online]. Georgia: Jamestown Foundation. Available: https://jamestown.org/program/georgias-civilizational-dilemma/ [Accessed 4 February 2025].

SHNEOR, R., CAMGÖZ, S. M. & KARAPINAR, P. B. 2017. The interaction between culture and sex in the formation of entrepreneurial intentions. *Cultural Values and Entrepreneurship.* Routledge. https://doi.org/10.1080/08985626.2013.862973

TOFALLIS, C., DUNK, T. & SPENCER, N. H. 2022. A multidimensional ranking of Members of Parliament. *Radical Statistics,* 133**,** 1-27. http://dx.doi.org/10.2139/ssrn.4465335

UNITED, N. 2023. *Concerned by Restrictions on Religious Freedom, Speakers Warn against Using Religion to Fuel Conflict, as Security Council Considers Situation in Ukraine* [Online]. International Court of Justice. Available: https://press.un.org/en/2023/sc15178.doc.htm [Accessed 4 February 2025].

WENNBERG, K., PATHAK, S. & AUTIO, E. 2013. How culture moulds the effects of self-efficacy and fear of failure on entrepreneurship. *Entrepreneurship Regional Development,* 25**,** 756-780. https://doi.org/10.1080/08985626.2013.862975

ISSN 1582-1021
e-ISSN 2668-4764
Edited by "AUREL VLAICU" University of Arad Publishing House, Arad, Romania

10.62591/Scien.Tech.Bull-Chem.FoodSci.Eng.2024.21.01

Article

PARTICULATE MATTER (PM1, PM2.5, PM10) MONITORING IN INDOOR AND OUTDOOR ENVIRONMENTS AT "AUREL VLAICU" UNIVERSITY OF ARAD, ROMANIA

Andreea-Corina MARCU[1], Lorena Aliana Ioțcu[2], Lucian Octav COPOLOVICI[1,2], Dorina Rodica CHAMBRE[1,2*]

[1]Faculty of Food Engineering, Tourism and Environmental Protection, "Aurel Vlaicu" University, Romania, 2 Elena Dragoi, Arad 310330, Romania
[2] Interdisciplinary Doctoral School of Aurel Vlaicu University, 2 Elena Dragoi, Arad 310330, Romania
Corresponding author email: dorinachambree@yahoo.com

Abstract: *The presence of particulate matter, along with other specific air pollutants, significantly contributes to the degradation of air quality outdoors and indoors. High concentrations of PM in indoor educational spaces influence students' health and daily performance. This study presents the results of daily monitoring of PM1, PM2.5, and PM10 concentrations carried out between May 9 and May 15, 2024, at 8:00, 10:00, 12:00, 14:00, and 16:00 in various indoor environments of the M University Complex at "Aurel Vlaicu" University of Arad, including two corridors, two student laboratories, and an auditorium, as well as in the outdoor environment. For indoor environment, the findings indicated relatively low levels of particulate matter, suggesting good air quality for student health with average PM1 concentrations ranged from 2 µg/m³ to 6 µg/m³, PM2.5 from 4 µg/m³ to 11 µg/m³, and PM10 from 5 µg/m³ to 14 µg/m³.*

Keywords: particulate matter, indoor air, outdoor environments, pollutants source, air quality

INTRODUCTION

Air pollution has long been a significant concern, not only due to its environmental impact but also because of its effects on human health. In addition to monitoring outdoor air quality (atmospheric air), indoor air quality (IAQ) requires particular attention, as people spend approximately 70-80% of their time in enclosed spaces, where the potential for exposure to indoor pollutants is high (Kozielska et al., 2020). According to the World Health Organization (WHO), indoor air pollution is the principal cause of Sick Building Syndrome (SBS) associated with pulmonary and respiratory deficiencies (Mansor et al., 2024). In situations involving non-compliant ventilation systems, inadequate room ventilation, and the presence of various indoor pollution sources (e.g., furniture, smoking, carpets, cleaning agents, hygiene products, construction materials, and heating systems), pollutants can accumulate in high concentrations potentially causing adverse effects on human health (Coggins et al., 2024; Tran et al., 2020; Yasmin et al., 2024). Many studies have shown that indoor air pollution can lead to cardiovascular, ocular, olfactory, respiratory, and pulmonary diseases (Abdel-Salam, 2022; Mulia et al., 2020; Sadrizadeh et al., 2022) or even affect the endocrine system by increasing the production of stress hormones, thus affecting the hypothalamic-pituitary-ovarian axis and menstrual function (Giorgis-Allemand et al., 2020; Wronka and Kliś, 2022). Recent studies pay special attention to young people, such as pupils and students, who participate in educational activities (Fang et al., 2023; Kanama et al., 2023; Mulia et al., 2020; Ongwandee et al., 2024; Sadrizadeh et al., 2022). These individuals spend approximately 30% of their day at school and 70% of their time indoors (e.g., classrooms, auditoriums, laboratories, etc.) (Zhu et al., 2021). Young people are more vulnerable to poor IAQ than adults due to their immature organs, lower pulmonary capacity, and higher breathing rates associated with physical activity (Font-Ribera et al., 2022). Poor IAQ can negatively affect their academic performance and daily behavior (Fang et al., 2023; Grineski et al., 2019). Therefore, ensuring a valuable IAQ in educational spaces is of great importance. It is demonstrated that, together with other specific air pollutants (i.e., CO, CO_2, SO_2, NOx, HCOH, VOCs, etc.),

particulate matter (PM) stands out for its negative contribution to air quality. These suspended airborne particles can have different sizes, showing different behaviour. The particulate matter resulting from natural sources have diameters between 1μm (PM1) and 10 μm (PM10) and contain dust, sea salts and bioaerosols etc., while those resulting from anthropogenic activities (e.g. fuel combustion, transport, construction, smoking, cooking, agriculture, industry, etc.) vary between 0.1μm (PM0.1) and 2.5 μm (PM2.5) and contain compounds such as sulphates, ammonium nitrates, elemental carbon, metals and heavy metals, organic structures, etc. (Fromme et al., 2008; Mansor et al., 2024; Tang and Pfrang, 2023).

According to Son et al. (Son, 2023), inadequate ventilation is the main factor contributing to high PM levels in enclosed spaces destined for educational activities. In schools, the reliance on natural ventilation facilitates the transport of pollutants from the outdoors into the indoor environment, especially in classrooms (Diapouli et al., 2008; Zhu et al., 2021). Rovelli et al. reported poor IAQ in classrooms in northern Italy due to high concentrations of airborne particulate matter (Rovelli et al., 2014). Recent studies indicate that among the various air pollutants found in classrooms, fine particulate matter with a diameter of 2.5 μm (PM2.5) poses a significant threat to the health of students (Kim et al., 2015; Ongwandee et al., 2024; Sadrizadeh et al., 2022; Son, 2023; Zhu et al., 2021).

Inside classrooms and university auditoriums, high values of PM2.5 and PM10 are caused by various factors such as indoor activities, use of chalk and other teaching materials, deterioration of building materials, emissions of small particles from furniture, heating systems, resuspension (due to the movement of students from one place to another) of material particles deposited in the dust form, air flow from outside, etc. (Dorizas et al., 2014; Elbayoumi et al., 2014; Fromme et al., 2008; Guo et al., 2010). These particles can easily penetrate the respiratory system, favoring the development of pulmonary diseases (Wichmann et al., 2010). They can also favor ocular and olfactory dysfunctions (Sadrizadeh et al., 2022; Son, 2023) or exacerbate the symptoms of atopic dermatitis (Kim et al., 2015).

Monitoring the IAQ and PM values of indoor educational spaces has become necessary to ensure healthy conditions for developing activities.

The purpose of this study is to measure PM1, PM2.5 and PM10 concentrations (μg/m^3) in different indoor and outdoor environment at "Aurel Vlaicu" University of Arad, Romania (University Complex M.) and estimate the air quality in educational spaces.

MATERIALS AND METHODS

PM1, PM2.5, and PM10 concentration measurements were carried out in five indoor locations at the M. University Complex of "Aurel Vlaicu" University of Arad (2 E. Drăgoi Str.) and outside this location. The sampling locations are as follows:

L1- outdoor environment of University Complex M

L2 - building access corridor located on the ground floor with a direct opening to the outside

L3 - 1st floor corridor, ventilation through windows

L4 - Chemistry-Physics laboratory located at 1st floor, with ventilation through windows

L5 - Environmental Protection laboratory, located at 1st floor, with ventilation through windows

L6 - "Dimitrie Cameniță" auditorium located on the ground floor, with a ventilation system in the room's upper part (ceiling).

The particulate matter concentrations were carried out using the professional air analyzer Dienmern DM 106 (Shenzhen Dienmern Testing Technology Co., Ltd., Guangdong, China) with a detection limit of 1 μg/m^3, during the May 9 – May 15, 2024, period, between 8:00-16:00 (sampling times: 8:00, 10:00, 12:00, 14:00, 16:00). The used analyzer had a built-in laser dust counter, dust sensor and time/date indicator, being able to measure PM1, PM2.5, PM10, HCHO, TVOC concentrations, air temperature as well as air humidity. The sample was taken at a height of approximately 1.5 meters above the ground or

floor. For each measurement, a time of ~10 min. was allocated in order to stabilize the displayed values. Microsoft Excel was used for the graphic representation.

RESULTS AND DISCUSSIONS

The analysis of the experimental data obtained involved the interpretation of the average PM concentrations from each sampling location at different monitored times. The average concentration values (µg/m^3) for particulate matter PM1, PM2.5, and PM10 in the monitored indoor locations are presented in Fig.1, Fig.2, and Fig.3.

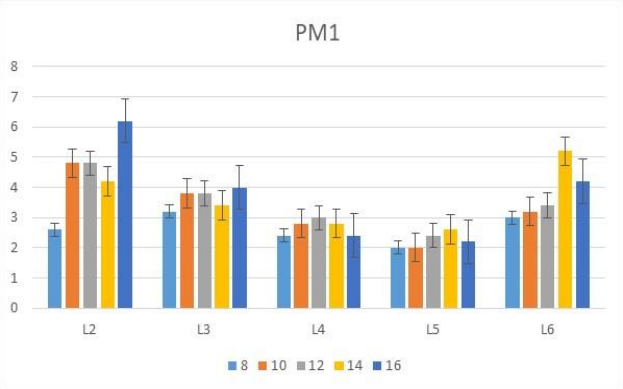

Figure 1. Average values of PM1 concentrations (µg/m^3) in the indoor locations L2, L3, L4, L5, L6 (M. University Complex, "Aurel Vlaicu" University of Arad)

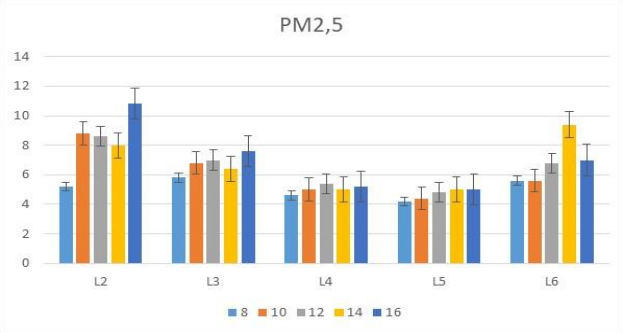

Figure 2. Average values of PM2.5 concentrations (µg/m^3) in the indoor locations L2, L3, L4, L5, L6 M. University Complex, "Aurel Vlaicu" University of Arad)

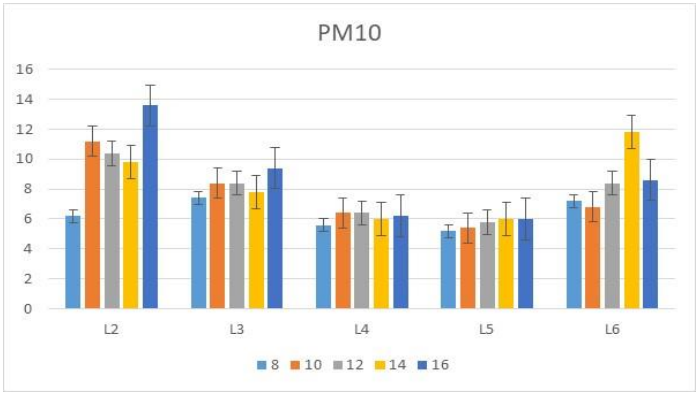

Figure 3. Average values of PM10 concentrations (µg/m^3) in the indoor locations L2, L3, L4, L5, L6 (M. University Complex, "Aurel Vlaicu" University of Arad)

From Fig. 1, Fig. 2, and Fig. 3. it can be seen that the average concentration values (µg/m^3) obtained for 5 days in the monitoring interval time (times: 8:00, 10:00, 12:00, 14:00, 16:00) were the lowest for PM1 and the highest for PM10 with the following sequence:

PM1 <PM2.5<PM10.

The data indicate that the values obtained for all three types of particulate matter (PM1, PM2.5, PM10) remain relatively stable during the 8:00–16:00 time interval in locations L4 and L5. In contrast, this trend is not observed in locations L2 and L3, the two corridors, where particulate matter concentrations show significantly higher fluctuations and elevated values than those recorded in the L4 and L5 laboratories. These variations are primarily attributed to the high foot traffic in these areas and the influence of air currents from outside, which can introduce suspended particles from the external environment. The elevated concentration values in location L2, the main access hall connecting the street to the M. University Complex, can be explained by its daily use by approximately 500–700 people on average.

In location L5, the average PM1 concentrations remained stable throughout the monitored time interval, ranging between 2 µg/m^3 and 3 µg/m^3. A similar pattern was observed for PM2.5, with average concentrations ranging from 4 µg/m^3 up to 5 µg/m^3. Slightly higher but relatively consistent values were recorded for PM10, ranging between 5 µg/m^3 and 6 µg/m^3 in location L5.

The average PM concentration values observed in location L5 can be attributed to a lower number of students (particularly on Fridays and during the morning times of 8:00 to 10:00) as well as to the recent modernization of this laboratory. The laboratory has been equipped with new furniture, and the relatively small number of chemical containers present are stored under appropriate conditions. This difference becomes much more visible when the data from location L5 are compared with those from location L4. Despite being on the same floor and exposed to a similar daily number of students, the average PM1, PM2.5, and PM10 concentrations in L4 were higher than in L5. This is likely attributable to L4 being furnished with older equipment, lacking recent renovations, and improper storage of chemicals.

In location L6 (the "Dimitrie Cameniță" auditorium), high average concentrations of the three PM types and significant daily fluctuations were observed. Notably, the highest PM10 value across all monitored locations during the entire period was obtained here: 25 µg/m^3 on May 14, 2024, at 14:00. The elevated PM concentrations in this location can be attributed to the large number of students using the auditorium, the use of teaching materials such as the chalkboard, and the construction materials from the walls and ceiling which tend to accumulate particles indoors in the absence of proper ventilation.

A comparison of the average PM concentrations shown in Fig. 1, Fig. 2, and Fig. 3 reveals that the highest values were recorded in location L2 (ground floor access hall) at 14:00, followed by location L6 ("Dimitrie Cameniță" auditorium) at 16:00 for all three types of monitored particles.

Reported data on air quality in classrooms and lecture halls indicate average PM1 values of approximately 2–16 µg/m³, PM2.5 values of approximately 5–24 µg/m³ and PM10 values of approximately 20–160 µg/m^3 (Sadrizadeh et al., 2022; Son, 2023; Diapouli et al., 2008; Zhu et al., 2021).

Compared to the findings reported in various scientific studies (Kim et al., 2015; Ongwandee et al., 2024; Sadrizadeh et al., 2022; Son, 2023; Zhu et al., 2021), the average PM1, PM2.5, and PM10 concentrations in the indoor monitored locations at "Aurel Vlaicu" University of Arad are considerably lower. These results indicate excellent air quality and a healthy environment within the educational spaces of the M. University Complex. It is mentioned that globally no mandatory standards exist for PM2.5 and PM10 concentrations in indoor air. However, WHO guidelines are most commonly used to assess indoor air quality. These guidelines establish reference values based on health impacts: for PM2.5, an annual average of 10 µg/m³ and a maximum of 25 µg/m³ for 24-hour exposure are recommended, while for PM10, the recommended values are 20 µg/m³ as an annual average and 50 µg/m³ for 24-hour exposure (https://www.who.int/publications/i/item/9789240034228).

Fig.4. shows the average values of PM1, PM2.5, and PM10 concentrations obtained during the monitored period for the outdoor environment (L1 location) of the M University Complex.

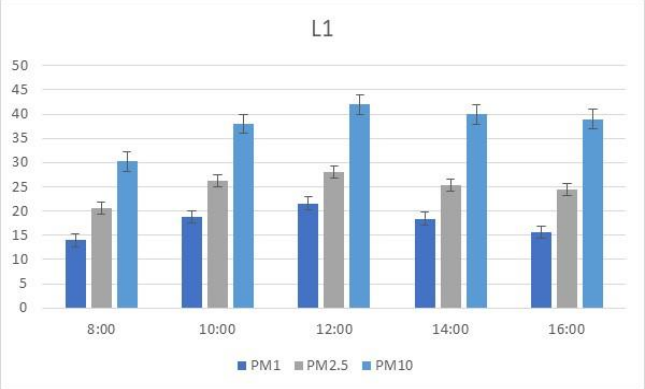

Figure 4. Average PM concentration values (µg/m³) obtained for the outdoor location L1 (M. University Complex, "Aurel Vlaicu" University of Arad)

From Fig. 4, it can be seen that the average concentrations obtained for PM1, PM2.5, and PM10 in the L1 location from the outdoor environment are considerably higher than those obtained in indoor L2, L3, L4, L5, and L6 (see Fig.1, Fig.2 and Fig.3) as expected. For PM1, the values ranged from 14 µg/m³ to 21 µg/m³; for PM2.5, they ranged from 21

µg/m³ to 27 µg/m³; and for PM10, the values varied between 30 µg/m³ and 41 µg/m³. These values do not exceed the limit values allowed by the legislation in force according to which "the concentrations of suspended particles with a diameter of less than 10 microns in the ambient air are evaluated by relating them to the daily limit value, (50 µg/m^3), which must not be exceeded more than 35 times/year and the annual limit value, (45 µg/m^3 for PM10 and 25 µg/m^3 for PM2.5)" (Law no 104/15.06.2011 on the quality of the surrounding air; Directive no. 2008/50/CE of EP). A correlation can be observed between the average concentration values obtained in locations L1 and L2, which supports the hypothesis that the outdoor air quality also influences the air quality in the indoor access hall.

CONCLUSIONS

From May 9 to May 15, 2024, concentrations of PM1, PM2.5, and PM10 were monitored at five indoor locations within the M University Complex at "Aurel Vlaicu" University of Arad, including two corridors, two student laboratories, and one auditorium, at 8:00, 10:00, 12:00, 14:00, and 16:00. The results revealed relatively low levels of particulate matter, indicating good air quality for student health. Average PM1 concentrations ranged from 2 µg/m³ to 6 µg/m³, PM2.5 from 4 µg/m³ to 11 µg/m³, and PM10 from 5 µg/m³ to 14 µg/m³. The indoor particle concentrations were lower than those recorded outdoors.

The indoor particulate matter (PM) concentrations were significantly influenced by the level of foot traffic and the number of students occupying each space, as these factors contribute to the resuspension of dust and particles within the indoor environment. Additionally, several other factors played a notable role in shaping the measured concentrations. The use of various teaching materials during classes often generates fine particulate matter. At the same time, old furniture and outdated equipment may act as sources of particle release over time, especially if poorly maintained. The lack of recent renovations further exacerbates this issue, as aging infrastructure accumulates dust and deterioration, releasing particles into the air. Improper chemical storage, particularly in laboratory or storage spaces, can also contribute to particulate matter levels through chemical reactions or the volatilization of certain compounds. Finally, outdoor air currents entering through open windows, doors, or ventilation systems can introduce suspended particles from the external environment, adding to indoor PM concentrations. These combined factors underscore the complexity of maintaining optimal indoor air quality in educational settings.

REFERENCES

Abdel-Salam, M.M.M., 2022. Relationship between residential indoor air quality and socioeconomic factors in two urban areas in Alexandria, Egypt. Building and Environment 207, 108425.

Coggins, A.M., Hogan, V., Mishra, A.K., Norton, D., Foster, D., Wemken, N., Cowie, H., Doherty, E., 2024. Energy retrofits: Factors affecting a just transition to better indoor air quality. Indoor Environments 1, 100058.

Diapouli, E., Chaloulakou, A., Mihalopoulos, N., Spyrellis, N., 2008. Indoor and outdoor PM mass and number concentrations at schools in the Athens area. Environmental monitoring and assessment 136, 13-20.

Dorizas, P., Assimakopoulos, M., Helmis, C., Santamouris, M., 2014. An integrated evaluation study of the ventilation rate, the exposure and the indoor air quality in naturally ventilated classrooms in the Mediterranean region during spring. The Science of the total environment 502C, 557-570.

Elbayoumi, M., Ramli, N.A., Md Yusof, N.F.F., Yahaya, A.S.B., Al Madhoun, W., Ul-Saufie, A.Z., 2014. Multivariate methods for indoor PM10 and PM2.5 modelling in naturally ventilated schools buildings. Atmospheric Environment 94, 11-21.

Fang, Y., Luo, X., Lu, J., 2023. A review of research on the impact of the classroom physical environment on schoolchildren's health. Journal of Building Engineering 65, 105430.

Font-Ribera, L., Rico, M., Marí-Dell'Olmo, M., Oliveras, L., Trapero-Bertran, M., Perez, G., Valero, N., Bartoll, X., Realp, E., Gomez,

A., 2022. Estimating ambient air pollution mortality and disease burden and its economic cost in Barcelona. Environmental Research 216, 114485.
Fromme, H., Diemer, J., Dietrich, S., Cyrys, J., Heinrich, J., Lang, W., Kiranoglu, M., Twardella, D., 2008. Chemical and morphological properties of particulate matter (PM10, PM2.5) in school classrooms and outdoor air. Atmospheric Environment 42, 6597-6605.
Giorgis-Allemand, L., Thalabard, J.C., Rosetta, L., Siroux, V., Bouyer, J., Slama, R., 2020. Can atmospheric pollutants influence menstrual cycle function? Environmental Pollution 257, 113605.
Grineski, S., Collins, T., Adkins, D., 2019. Hazardous air pollutants are associated with worse performance in reading, math, and science among US primary schoolchildren. Environmental Research 181, 108925.
Guo, H., Morawska, L., He, C., Zhang, Y., Ayoko, G., Cao, M., 2010. Characterization of particle number concentrations and PM2.5 in a school: Influence of outdoor air pollution on indoor air. Environmental science and pollution research international 17, 1268-1278.
Kanama, N., Ondarts, M., Guyot, G., Outin, J., Golly, B., Gonze, E., 2023. Effect of energy renovation on indoor air quality and thermal environment in winter of a primary school in a highly polluted French alpine valley. Journal of Building Engineering 72, 106529.
Kim, E.-H., Kim, S., Lee, J.H., Kim, J., Han, Y., Kim, Y.-M., Kim, G.-B., Jung, K., Cheong, H.-K., Ahn, K., 2015. Indoor Air Pollution Aggravates Symptoms of Atopic Dermatitis in Children. PLOS ONE 10, e0119501.
Kozielska, B., Mainka, A., Żak, M., Kaleta, D., Mucha, W., 2020. Indoor air quality in residential buildings in Upper Silesia, Poland. Building and Environment 177, 106914.
Mansor, A.A., Abdullah, S., Ahmad, A.N., Ahmed, A.N., Zulkifli, M.F.R., Jusoh, S.M., Ismail, M., 2024. Indoor air quality and sick building syndrome symptoms in administrative office at public university. Dialogues in Health 4, 100178.
Mulia, G.J.T., Wispriyono, B., Kusnoputranto, H., Hartono, B., Rozaliyani, A., 2020. Indoor Air Pollution and Respiratory Function on Primary School Students in West Jakarta, Indonesia. The Open Public Health Journal 13, 190-195.
Ongwandee, M., Khianthongkul, K., Panyametheekul, S., Yongprapat, K., Srinaka, K., Morris, J., 2024. Bangkok school indoor air quality: monitoring and intervention by positive pressure fresh air system. Environmental Science and Pollution Research 31, 1-14.
Rovelli, S., Cattaneo, A., Nuzzi, C.P., Spinazzè, A., Piazza, S., Carrer, P., Cavallo, D.M., 2014. Airborne Particulate Matter in School Classrooms of Northern Italy, International journal of environmental research and public health, pp. 1398-1421.
Sadrizadeh, S., Yao, R., Yuan, F., Awbi, H., Bahnfleth, W., Bi, Y., Cao, G., Croitoru, C., de Dear, R., Haghighat, F., Kumar, P., Malayeri, M., Nasiri, F., Ruud, M., Sadeghian, P., Wargocki, P., Xiong, J., Yu, W., Li, B., 2022. Indoor air quality and health in schools: A critical review for developing the roadmap for the future school environment. Journal of Building Engineering 57, 104908.
Son, Y.-S., 2023. A review on indoor and outdoor factors affecting the level of particulate matter in classrooms of elementary schools. Journal of Building Engineering 75, 106957.
Tang, R., Pfrang, C., 2023. Indoor particulate matter (PM) from cooking in UK students' studio flats and associated intervention strategies: evaluation of cooking methods, PM concentrations and personal exposures using low-cost sensors. Environmental Science: Atmospheres 3, 537-551.
Tran, V.V., Park, D., Lee, Y.C., 2020. Indoor Air Pollution, Related Human Diseases, and Recent Trends in the Control and Improvement of Indoor Air Quality. International journal of environmental research and public health 17.
Wichmann, J., Lind, T., Nilsson, M.A.M., Bellander, T., 2010. PM2.5, soot and NO2 indoor–outdoor relationships at homes, pre-schools and schools in Stockholm, Sweden. Atmospheric Environment 44, 4536-4544.
Wronka, I., Kliś, K., 2022. Effect of air pollution on age at menarche in polish females, born 1993–1998. Scientific Reports 12, 4820.

Yasmin, A., Ahmed, I., Haider, M., Hossain, M.K., Motalib, M.A., Hossain, M.S., 2024. Characterizing indoor air quality and identifying factors influencing air quality at home microenvironment in Dhaka city. Indoor Environments 1, 100056.
Zhu, Y.-D., Li, X., Fan, L., Li, L., Wang, J., Yang, W.-j., Wang, L., Yao, X.-y., Wang, X., 2021. Indoor air quality in the primary school of China—results from CIEHS 2018 study. Environmental Pollution 291, 118094.

ISSN 1582-1021
e-ISSN 2668-4764
Edited by "Aurel Vlaicu" University of Arad Publishing House, Arad, Romania

10.62591/Scien.Tech.Bull-Chem.FoodSci.Eng.2024.21.02

ASSESSMENT OF SURFACE WATER QUALITY IN JIU VALLEY MINING AREA

Carmen ROBA[1], Liliana MANULESC[1], Delia GLIGOR[1*]

[1] Faculty of Environmental Science and Engineering, Babeş-Bolyai University, 30 Fantanele Street, RO-400294, Cluj-Napoca, Romania
[*]Corresponding author email: delia.gligor@ubbcluj.ro

***Abstract**: The main objective of the present study was to perform a general screening of surface water quality in Jiu Valley mining rea. Surface waters were collected from West Jiu river and some of its tributaries (Căprişoara creek; Baleia creek; Bărbăteni creek; Vacii Valley creek; Tusu creek; Bulzu creek) to analyze several general physico-chemical and some specific chemical quality parameters. The general physico-chemical parameters: pH, redox potential (ORP), salinity, total dissolved solids (TDS), electrical conductivity (EC) and dissolved ions were analyzed.*

The analyzed water samples had a neutral pH, with a relatively low content of dissolved salts, except for Căprişoara creek. Based on their dissolved ions content, most of the analysed waters correspond to Ist quality class, which reflect a very good ecological status. Because of the high content of sulphate, calcium and magnesium, water sampled from Căprişoara creek corresponds to Vth class (based on SO_4^{2-} content), IVth class (Ca^{2+} level) and IIIrd (Mg^{2+} concentration) class, indicating a bad / low / moderate ecological status. The water quality degradation of Căprişoara creek in the investigated area may be associated with several anthropic activities identified in the area, but to confirm this sources further investigations are needed.

Keywords: Jiu Valley, mining units, water quality.

INTRODUCTION

Degradation of surface water quality due to anthropogenic activities (agriculture, industry, urbanization, deforestation, etc.) or natural factors (soil erosion, meteorological phenomenon-rain, climate change, etc.) represents a global problem (Munabi et al., 2009). Surface water pollution leads to equilibrium perturbation of the ecosystem and can have a negative impact on public health (Dalakoti et al., 2017).

Mining industry represents one of the most important pollution sources of the environment, generating high amounts of waste during ore extraction, processing, transport and deposition. It can have a major impact on the landscape, soil or surface and underground water quality, leading to aquatic and terrestrial ecosystems degradation (Fodor, 2006). Generally, the mining activities are associated with four major effects on the environment, as was mentioned by Rybicka (1996): (i) changes in hydrogeological system; (ii) hydrological modifications of soils and surface water flux; (iii) contamination of soils and surface water basins and (iv) atmosphere pollution. The additional impacts are: reduced biodiversity, modifications of ecosystem functioning and structure, modifications of soil stratigraphy (Almas et al. 2004; Jason, 2012).

The present study was performed in a former mining area from Romania, namely in the mining basin of Jiu Valley, where the largest coal deposit from Romania was exploited during the XIX century. The extraction technologies used in the Jiu Valley were adapted to the geological mining characteristics, being conditioned, first of all, by the thickness and slope of the layer (Neagu et al., 2015). In 1840 the first surface operations began in the area, by the exploitation and coal processing within the Vulcan, Petroşani and Petrila mines (Faur et al., 2017). Coal exploitation intensified over time in the area, so that at the beginning of the '90s there were 14 mine perimeters put into operation in the Jiu Valley. The coal production declined in the area since 1996, when started the restructuring process (closure of some mining

units), the decline accelerating after 2000 in the area. Because of the lack of a visionary policy in the energy sector, the future of coal exploitation in Jiu Valley is uncertain (Faur et al., 2017).

Due to the intense mining activities carried out in the area in the past, it is possible that the environment is still facing a negative impact caused by the discharge of improperly treated wastewater, or by the hydrotechnical activities performed for permanent or torrential water courses regularization in interior or exterior of the mining perimeter, or by the leaching from the cool deposit (Almas et al., 2004; Jason, 2012).

The main objective of the present study was to perform a general screening of surface water quality in Jiu Valley mining rea. Surface waters were collected from West Jiu river and some of its tributaries (Căprișoara creek; Baleia creek; Bărbăteni creek; Vacii Valley creek; Tusu creek; and Bulzu creek) to analyze several general physico-chemical and some specific chemical quality parameters.

STUDY AREA

The investigated area is located in Hunedoara County, in the coal mining perimeter of Jiu Valley, Petroșani depression. A total of seven surface water samples were collected in October 2020 (Fig. 1). The sampling points are located on three territorial administrative units, respectively: Uricani, Lupeni and Vulcan.

Uricani town is located in the north of Jiu Valley, with Brazi Valley and Câmpu lui Neag as component localities. Uricani town was part of the Jiu Valley coal basin, located in its western part and bounded by the former mining perimeters from Bărbăteni (east) and Brazi Valley (west), having an area of 1548.6 ha. Currently, the Uricani mine is closed, as remedial and reintegration activities have been started in the natural landscape of the area occupied by the constructions specific to the activities of the past (Buliga, 2017).

Lupeni mining perimeter is located in the central-western part of the Petroșani depression, being adjacent to the east of the Vulcan mining perimeter and to the west of the former Bărbăteni mining field. The mining perimeter has an area of 1334.7 ha, where the Lupeni Mining Exploitation operates, whose object of activity is the extraction of energy coal contained in layer 3 (Buliga, 2017). The main water course is represented by West Jiu, which collects the tributaries from the slopes of the depression. The water samples were taken mainly from the areas downstream from the mining units or fields, respectively the samples from Pâraiele Tusu (sample no. 6) and Vacii Valley (sample no. 5), being downstream from the former exploitations from Uricani, the sample from the Bărbăteni stream (sample no. 4) being taken from downstream of the former Bărbăteni exploitation.

Figure 1. Location of the surface water sampling points – Jiu Valley mining area (1 – West Jiu river; 2 – Căprișoara creek; 3 – Baleia creek; 4 – Bărbăteni creek; 5 – Vacii Valley creek; 6 – Tusu creek; 7 – Bulzu creek) (modified after Google Erath).

Vulcan mining perimeter is located in the central area of the West Jiu Valley and covers an area of 12.6 km^2. Vulcan perimeter is bounded to the east by the Aninoasa mining perimeter, and to the west by the Paroșeni and Lupeni mining perimeters. The mining activity is managed by Hunedoara Energetic Complex S.A. Company. At the level of 2014, the Vulcan mine had two production sectors, one electro-mechanical sector, one transport sector and a ventilation sector (Buliga, 2017). In addition to the DN 66A national road, access to the premises is via the Petroșani-Livezeni-Lupeni railway. The hydrographic network in the described perimeter is tributary to the West Jiu River. Samples

were collected from tributaries of the Jiu River that either cross areas affected by both current and historical mining activities or affected by industrial activities such as the Paroșeni thermal power plant. As it can be observed in Fig. 1, the samples were taken both upstream (upstream-sample no. 2 Căprișoara creek) and downstream of the mining units (downstream E.M. Lupeni- sample no. 3, Baleia creek and E.M. Vulcan- sample no. 1 Jiu).

MATERIALS AND METHODS

With the help of the multiparameter WTW Multi 350i, the following physico-chemical parameters were measured *in situ*: electrical conductivity (EC), total dissolved solids (TDS), salinity, pH, redox potential (ORP). Before the field measurements, the equipment was calibrated using standard buffer pH solutions (pH = 4.01; 7.00; 10.01) and standard solution with an electric conductivity of 1278 µS/cm (20°C), respectively 1413 µS/cm (25°C).

The samples destinated for major dissolved ions analyses were collected in sterile polyethylene vials, with a volume of 120 ml. The collection and preservation of water samples was carried out according to national and international standards (ISO 5667-1/2023, ISO 5667-3/2024). The samples were filtered in the field by using syringe filters with pore size of 0.45 µm. The vials were labelled and transported to the laboratory in dark at cold (5°C) condition. The analyses were performed within 48h from sampling by using an ion chromatography system (model IC 1500 Dionex – SUA), which allows the analyse of the following ions F^-, Cl^-, Br^-, NO_3^-, NO_2^-, SO_4^{2-}, PO_4^{3-}, Li^+, Na^+, K^+, NH_4^+, Ca^{2+}, and Mg^{2+}. The qualitative analysis was performed based on retention times for each ion present in the standard solution, while the quantitative analysis was carried out based on the external standard method, using the previously calibration curves plotted for each ion. The sensitivity of IC method was estimated based on the limit of detection (LOD) and the limit of quantification (LOQ). The results showed that ion chromatographic method had an adequate sensitivity, the LOD values ranged between 0.001 and 0.02 mg/l, and the LOQ values were in the range of 0.003 – 0.065 mg/l, depending on the ion. The limit of detection (LOD) and the limit of quantification (LOQ) were calculated based on the standard deviation of the response – σ (10 repeated measurements of the blank sample) and the slope of the calibration curve – S, according to the formulas below:

$$LOD = \frac{3.3\times\sigma}{S}\,;\; LOQ = \frac{10\times\sigma}{S}$$

The content of carbonates and bicarbonates was measured by titration with HCl, in the presence of phenolphthalein and methylorange as indicators.

RESULTS AND DISCUSSIONS

Determination of physico-chemical parameters

Seven surface water samples were taken from the mining perimeter of Jiu Valley, in order to determine their physico-chemical parametes (the values are presented in Table 1).

Table 1. Values of physico-chemical parameters for the collected surface water samples

Sample	pH	ORP (mV)	EC (µS/cm)	TDS (mg/l)	Sal. (‰)
1. West Jiu river	7.74	-61.9	175.1	112	<0.01
2. Căprișoara creek	7.48	-49.5	665.0	425	0.3
3. Baleia creek	7.57	-54.4	68.2	44	<0.01
4. Bărbăteni creek	7.62	-55.1	192.0	123	<0.01
5. Vacii Valley creek	7.80	-61.9	59.4	38	<0.01
6. Tusu creek	7.73	-60.3	97.5	62	<0.01
7. Bulzu creek	7.72	-61.2	122.4	78	<0.01

The pH indicates the hydrogen ions concentration, which determines the acid or basic character of water. The water pH change is related to the formation and decomposition processes of organic substances, on which the decrease or increase of carbonic acid concentration depends. The development and vital activity of aquatic organisms, as well as the

stability and migration of chemical elements depend on the pH (Puri, 2015). The analyzed water samples had a neutral pH (between 7.48 and 7.80) (Table 1), being within the limits (6.5 – 8.5) imposed by the national legislation (Order no. 161 from 16.02.2006).

The redox potential presented negative values (between -49.5 and -61.9 mV), being indirectly correlated with pH values. There are studies that have highlighted the correlation between the redox potential and the abundance of nitrate ion, namely the fact that the depletion of nitrite correlates with switching from a positive to negative ORP gradient (Weißbach et al., 2018). Therefore, the negative values of the potential could be a possible reason why the nitrite content in all the analysed samples was below the detection limit.

Electrical conductivity is an important parameter, being an indicator of the level of dissolved salts, including magnesium, sulphate, sodium, chloride, or calcium. Depending on EC values, the water can be used in irrigation, recreational, industrial or other purposes. The surface water samples had a low EC, between 68.2 and 665.0 µS/cm. The highest EC value was registered in Căprișoara creek, which has the confluence with West Jiu river, downstream of Vulcan mining exploitation area. Considering that surface water is an important resource for agriculture, the EC value of the investigated waters is suitable for agricultural usage. Generally, water with EC <750 µS/cm is safe so be used for irrigation (Kadhem, 2013).

The total dissolved solids TDS (mg/l) in water include, generally, inorganic salts (as carbonate, bicarbonate, chloride, sulphate, nitrate, sodium, potassium, calcium and magnesium) and a small quantity of organic material (Puri, 2015). Thus, the values for the total dissolved solids are between 38 mg/l for Vacii Valley creek and 425 mg/l for the sample number 2, collected from Căprișoara creek.

The analysed water samples had a low salinity, the values being below the detection limit of the equipment (<0.01‰), with the exception of Căprișoara creek, where the salinity was 0.3‰ (Table 1).

Ions concentration in surface water samples

Concentrations of dissolved ions for the investigated water samples are presented in Figure 2 and the quality classes can be determined according to the present legislation (Order no. 161 from 16.02.2006). The ions concentrations F^-, NO_2^-, Br^-, PO_4^{3-}, K^+, Li^+, NH_4^+ were under the detection limit of the equipment.

The distribution of major dissolved ions was dominated by the presence of SO_4^{2-}, HCO_3^-, Ca^{2+} and Mg^{2+} (Fig. 2). The surface waters had a low Cl^- content, between 0.91 and 7.04 mg/l, which corresponds to Ist quality class "very good ecological status". Similar to Cl^-, the NO_3^- content was low, the values for $N\_NO_3^-$ ranged between 0.09 – 0.51 mg/l, all the samples being classified as Ist quality class "very good ecological status". The nitrates content was slightly higher in samples 1-3 compared to the rest of the samples. Nitrates presence in surface waters can be associated with natural and anthropic sources (agriculture by manure elimination, food production and deposit activities of household and industrial waste) (Puri, 2015).

Except for sample no. 2, the sulphate content was low, corresponding to Ist quality class "very good ecological status" (Fig. 2). In sample 2, the sulphate was abnormally high, the water sample being classified as Vth quality class "bad ecological status". The high content of sulphate from Căprișoara creek (sample no. 2) reflected an anthropic impact, which can be correlated with possible leachate of pollutants from the household waste dumps located upstream from the sampling point, or with the aerial dispersion of pollutants from the surface of the ash pits generated by Paroșeni Plant, located at approximately 500 m from the sampling point. Therefore, through the action of rainwater, leachate appears, which can negatively influence the quality of underground and surface water from their perimeter. Further investigation is needed to assess the water quality of this particular tributary of West Jiu

river and to confirm the impact of the above mention anthropic activities.

High concentrations of SO_4^{2-} in surface water, can disturb the equilibrium and the ionic exchange processes, which can have a negative impact on aquatic organisms (Qian et al., 2017). Sulphates, sulfides and sulphurate hydrogen represent the sulphur combinations. Sulphates have a low stability, being a substrate for oxido-reduction bacteria and transform them into sulphurate hydrogen or soluble sulphides. Thus, in oxidation reactions, in the water presence, the sulfoxidant bacteria transform H_2S or elemental sulphur into sulphates. On the other hand, in reduction reactions, bacteria transform sulphates in H_2S which is obtained or in the iron presence can form pyrites FeS (Bech et al., 2017).

The carbonate was not detected in the analysed water, while the bicarbonate content ranged between 75 and 254 mg/l. The highest bicarbonate levels were registered in sample no. 1 – West Jiu river (150 mg/l) and in sample no. 2 – Căprișoara stream (254 mg/l). The presence of bicarbonates in surface waters can be correlated with the geological features of the aquifers, namely to the presence of limestone and dolomite. Thus, the presence of carbon in dolomite and calcite is responsible for the presence of almost half of the bicarbonate ions content from solution. The presence of these minerals determines an increase of calcium, magnesium and bicarbonate ions concentration in water (Gastmans et al., 2010; Khashogji et al., 2013). Possible sources for carbonates and bicarbonates in surface waters can include the presence of organic material in aquifer, which is oxidized and produces CO_2, favoring mineral dissolution.

The sodium content was low (between 0.89 and 6.87 mg/l) for the analysed surface water samples, corresponding to Ist quality class "very good ecological status" (Fig. 2). With the exception of sample no. 2, the rest of the samples had a low content of calcium and magnesium which correspond to Ist quality class "very good ecological status" and respectively to IInd quality class "good ecological status" (sample 1 for Mg^{2+} content). The sample no. 2, collected from Căprișoara creek had a considerably higher magnesium (classified as IIIrd quality class "moderate ecological status") and calcium content (classified as IVth quality class "low ecological status") (Fig. 2). Such high levels of calcium and magnesium may be associated with anthropic sources, but in order to identify possible sources further investigations are needed.

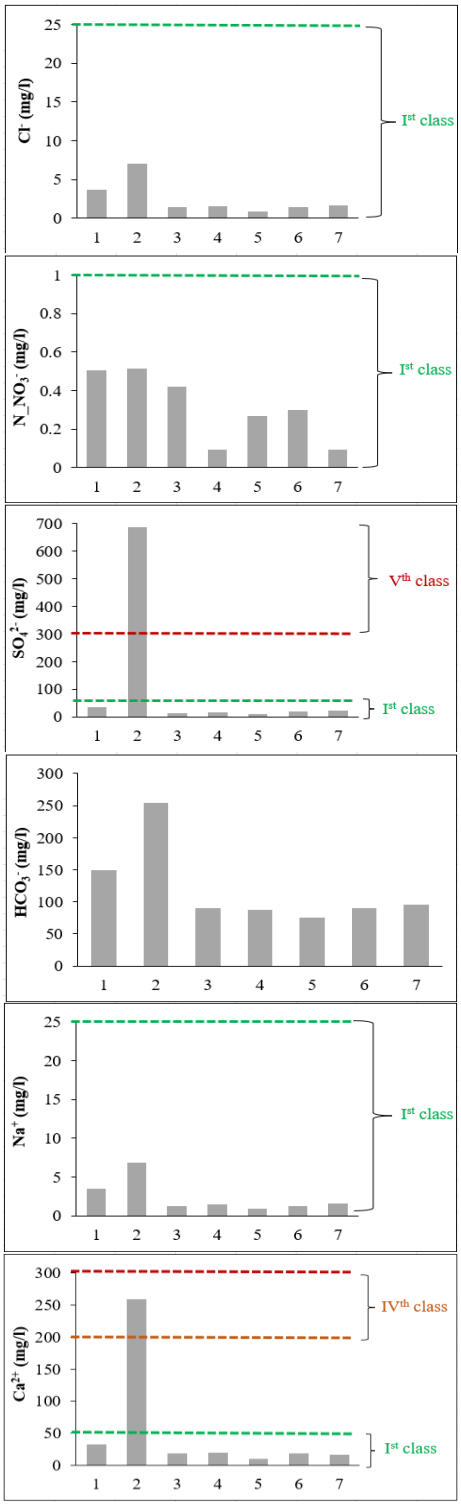

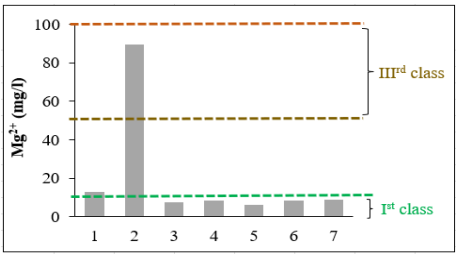

Figure 2. The content of major dissolved ions in the surface water samples and the corresponding water quality status according to national regulation (Order no. 161 from 16.02.2006).

Based on calcium and magnesium concentration, the water harness (HD) was calculated using the Water hardness calculator proposed by Lenntech. The results are presented in Fig. 3.

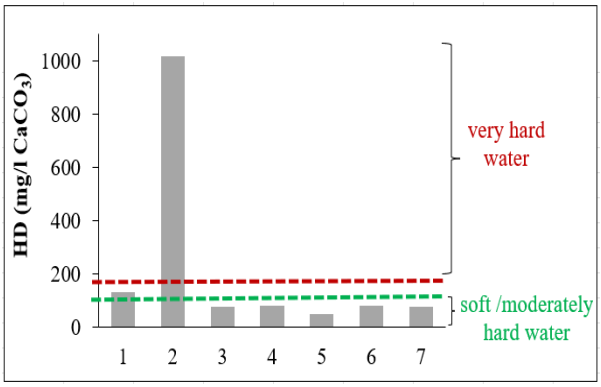

Figure 3. The hardness of the investigated surface waters.

Generally, the analysed waters can be classified as soft water (HD up to 60 mg/l $CaCO_3$) and moderately hard water (HD up to 120 mg/l $CaCO_3$). Sample no. 2 was again an exception, where the limit for very hard water (180 mg/l) was considerably exceeded. The water hardness from sample no. 2 - Căprișoara creek is caused by the high amount of dissolved calcium and magnesium salts in the water. Water hardness is a factor which restricts their usage in agriculture, industrial or recreational purposes. When passing through the pipes, the calcium and magnesium salts can form scale, which can reduce the life of equipment, raise the maintenance costs, lower the efficiency of electric water heaters, or lead to clog pipes. Too much salts in water used for irrigation can lead to accumulation of high amounts of salts in rootzone, which may reduce or even prohibit the crop production.

CONCLUSIONS

The main objective of this study was to evaluate the quality of surface water in the Jiu Valley, a mining area in southwest of Romania. Seven surface water samples crossing the territory of three territorial administrative units (Uricani, Lupeni, Vulcan) were analysed.

The analysed water samples had a neutral pH, with a relatively low content of dissolved salts, except for Căprișoara creek. Based on their dissolved ions content, most of the analysed waters correspond to Ist quality class, which reflect a very good ecological status. Căprișoara creek was an exception. Because of the high content of sulphate, calcium and magnesium, this water sample corresponds to Vth class (based on SO_4^{2-} content), IVth class (Ca^{2+} level) and IIIrd (Mg^{2+} concentration) class, indicating a bad / low / moderate ecological status. The contamination with these chemical compounds can be associated with possible anthropogenic sources, like leachate generated in the household waste dumps areas located upstream from the sampling point, or with the aerial dispersion of pollutants from the surface of the ash pits generated by Paroșeni Plant. To confirm this sources, further investigations are needed.

REFERENCES

ISO 5667-1:2023 Water quality. Sampling. Part 1: General guidance for sampling techniques

ISO 5667-3:2024 Water quality. Sampling. Part 3: Preservation and handling of water samples

Order 161 from 16 February 2006 Regulation on reference objectives for classifying surface water quality.

Almas, A.R., Bakken, L.R., Mulder, J., 2004. Changes in tolerance of soil microbial communities in Zn and Cd contaminated soils. Soil Biology and Biochemistry 805-813.

Buliga (Nălboc). I.V., 2017. The study of the impact on the environment of the pollutants generated by the mining units in the west of Valea Jiului. PhD thesis, University of Petroșani (in Romanian)
Dalakoti, H., Mishra, S., Chaudhary, M., Singal, S. K., 2017. Appraisal of water quality in the lakes of Nainital District through numerical indices and multivariate statistics, India. International Journal of River Basin Management 16, 1–11.
Faur, F, Marchiș, D, Nistor, C, 2017. Evolution of the coal mining sector in Jiu Valley in terms of sustainable development and current socio-economic implications. Research Journal of Agricultural Science 49 (4), 110-117.
Fodor, D., 2006. Influența industriei mineritului asupra mediului. Buletinul AGIR 3, 2-13.
Gastmans. D., Chang. H.K., Hutcheon. I., 2010. Groundwater geochemical evolution in the northern portion of the guarani aquifer system (Brazil) and its relationship to diagenetic features. Applied Geochemistry 25, 16–33.
Jason, P., 2012. Applying a mathematical model of sustainability to the Rapid Impact Assessment Matrix evaluation of the coal mining tailings dumps in the Jiului Valley, Romania. Resources, Conservation and Recycling 63, 17-25.
Kadhem, A.J., 2013. Assessment of Water Quality in Tigris River-Iraq by Using GIS Mapping Natural Resources 4, 441-448.
Khashogji. M.S., El Maghraby, M.M.S., 2013. Evaluation of groundwater resources for drinking and agricultural purposes, Abar Al Mashi area, south Al Madinah Al Munawarah City, Saudi Arabia. Arabian Journal of Geoscience 10, 3929–3942.
Lenntech, Water hardness calculator, https://www.lenntech.com/ro/water-hardness.htm.
Neagu, C., Bulearcă, M., Sima, C., Mărguș, D., 2015. A SWOT Analysis of Romanian extractive Iidustry and re-industrialization requirements of this industry. Procedia Economics and Finance 22, 287-295.
Munabi, C, Kansiime F, Amel A, 2009, Variation of water quality in Kakira catchment area, Jinja – Uganda. Physics and Chemistry of the Earth, Parts A/B/C 34 (13–16), 761-766.
Puri, P.J., Yenkie, M.K.N., Rana, D.B., Meshram S.U., 2015. Application of water quality index (WQI) for the assessment of surface water quality (Ambazari Lake), Pelagia Research Library 5(2), 37-52.
Qian, Z., Fen, G., Yuan, Z., Shuqin, M., Xiaobo, J., Wei, M., 2017. How sulfate-rich mine drainage affected aquatic ecosystem degradation in northeastern China, and potential ecological risk. Science of the Total Environment 1093-1102.
Rybicka, E.H., 1996. Impact of mining and metallurgical industries on the environment in Poland. Applied Geochemistry 11, 3-9.
Weißbach, M., Drewes, J.E., Koch, K., 2018. Application of the oxidation reduction potential (ORP) for process control and monitoring nitrite in a Coupled Aerobic-anoxic Nitrous Decomposition Operation (CANDO). Chemical Engineering Journal 343, 484-491.

ISSN 1582-1021
e-ISSN 2668-4764
Edited by "Aurel Vlaicu" University Publishing House, Arad, Romania

10.62591/Scien.Tech.Bull-Chem.FoodSci.Eng.2024.21.03

Article

BIOSYNTHESIZED GOLD NANOPARTICLES FROM *HEDERA HELIX* BIOMASS WASTE

Cristina Laura POPA[1,2], Cristian MOISA[1*], Andreea Ioana LUPITU[1], Lucian COPOLOVICI[1,3], Dana Maria COPOLOVICI[1,3]

[1] Institute for Interdisciplinary Research, "Aurel Vlaicu" University of Arad, 2 Elena Dragoi St., 310330 Arad, Romania.

[2] Biomedical Sciences Doctoral School, University of Oradea, 1 University St., 410087 Oradea, Romania.

[3] Faculty of Food Engineering, Tourism and Environmental Protection, "Aurel Vlaicu" University of Arad, 2 Elena Dragoi St., 310330 Arad, Romania.

Corresponding author email: moisa.cristian@yahoo.com

Abstract: *Hedera helix is an evergreen perennial vine plant often pruned for ornamental or ecological purposes. This process generates a significant amount of biomass waste. Therefore, this study aimed to use this biomass to obtain extracts rich in phenolic compounds and as a mediator for the biosynthesis of gold nanoparticles (AuNPs). Biochemical assays (DPPH, FRAP, Folin–Ciocalteu, and colorimetric determination of total flavonoid content) revealed that the extracts have significant radical scavenging activity and moderate phenolic and flavonoid compound levels. These findings were further supported by UHPLC analysis, providing insight into the chemical composition of these extracts. Only the most efficient extract (water infusion) was further used for AuNPs synthesis in three different synthesis medium concentrations of $HAuCl_4$ (0.5, 1, and 2 mM). Visual and UV-Vis spectroscopy analyses revealed the successful formation of AuNPs, while SEM-EDS analysis confirmed the morphology (spherical and polydisperse nanoparticles) and elemental composition. The antimicrobial activity was evaluated through the broth microdilution method against five microbial strains (Staphylococcus aureus, Escherichia coli, Salmonella typhimurium, Pseudomonas aeruginosa, and Candida albicans) and two antibiotics (penicillin and gentamicin). The resulting bacterial inhibition rate (BIR%) revealed a low inhibitory activity for AuNPs, significantly lower than for the tested antibiotics. It suggests that further AuNPs functionalizations may be required to increase their biological activity.*

Keywords: antimicrobial activity, gold nanoparticles, green synthesis, *Hedera helix*, phytochemical characterization.

INTRODUCTION

Throughout history, plants have played a crucial role in overcoming human ailments and diseases due to the biocompatibility of their secondary metabolites. These metabolites act as antioxidants, anticancer agents (Belmehdi et al., 2023; Mungwari et al., 2025), and antimicrobial substances with antibacterial and antifungal properties (Bezruk et al., 2020; Shokry et al., 2022; Vaou et al., 2021). However**,** unlike synthetic drugs, typically composed of single molecules, plant-based natural compounds are usually complex mixtures. These mixtures contain a vast array of chemicals (phenolic compounds, flavonoids, proteins, alkaloids, essential oils, saponins) (Belmehdi et al., 2023; Gavrila et al., 2023; Mungwari et al., 2025), some of which may have health benefits that haven't even been explored yet. Natural compounds' most significant advantages are that they often cause fewer side effects and work better within the organism, being highly biocompatible (Belmehdi et al., 2023; Shokry et al., 2022; Vaou et al., 2021).

The need to use ecologically derived plant compounds in green synthesis has recently opened new directions in nanotechnology (Sorbiun et al., 2018; Thipe et al., 2022). Using biological methods for synthesizing metal nanoparticles has the advantage of being low-cost and eco-friendly, and several plant-based compounds (alkaloids, terpenes, phenols, saponins, and proteins) can act as both reducing and stabilizing agents (Csakvari et al., 2021; Saravanan et al., 2021), making them the perfect candidates for green synthesis while lowering their overall toxicity and environmental impact (Thipe et al., 2022).

These resulting nanoparticles can often have therapeutic properties as antimicrobial agents (Belete, 2019), or they can further be used in obtaining biosensors or for several other applications in pharmacology and diagnostics (Rónavári et al., 2021; Sorbiun et al., 2018).

Hedera helix L., a member of the *Araliaceae* family, is a well-known climbing evergreen perennial vine plant native to a wide geographic range spanning western, central, and southern Europe, extending into northern Africa (Bezruk et al., 2020; Sen et al., 2023; Suica-Bunghez et al., 2020; Wyka et al., 2023). Documented records present an approximate length of over 30 meters, with robust shoots having a diameter of up to 25 centimeters forming a small trunk. The stems connect with the surrounding substrate through multiple leaf node roots, adhering to vertical surfaces like trees, on rocky cliffs similar to lianas, or creeping on the ground (Al-Snafi, 2018; Baharara et al., 2021; Suica-Bunghez et al., 2020). The leaves are colored in vibrant green shades, usually smaller than 8 cm, and present a particular smell when crushed. The flowers are small and organized in clusters of yellow-green color that lead to small drupe-like fruits containing between 2-5 seeds (Al-Snafi, 2018; Baharara et al., 2021).

Within the ivy plant, many phytochemicals are present, some of which are used in traditional medicine across various cultures. These compounds include saponins: α-hederin (Belmehdi et al., 2023; Gavrila et al., 2023; Shokry et al., 2022), hederacoside E and F, hederasaponin-C, flavonoids: quercetin, rutin, kaempferol, polyacetylenes, and phenolic compounds: caffeic acid, rosmarinic acid, *p*-coumaric acid, as well as amino acids, steroids, vitamins, and volatile and fixed oils (Al-Snafi, 2018; Suica-Bunghez et al., 2020). One of the traditional medicinal applications of *Hedera helix* was the preparation of a decoction from its leaves and fruits, used to treat coughs and other respiratory disorders (Al-Snafi, 2018; Baharara et al., 2021). In most of Europe's territories, ivy leaf extracts are still used in traditional treatments for most acute and chronic respiratory tract problems and inflammatory conditions (Shokry et al., 2022).

From a landscape perspective, common ivy is often integrated into vertical greenery systems and, due to its high biomass productivity, requires regular trimming, which results in the generation of substantial biomass waste (Vercruysse et al., 2024). The generated biomass trimmings have a rich chemical profile, containing various phytochemicals such as flavonoids, saponins, and essential oils, representing a promising and untapped source of natural capping and reducing agents essential for green nanoparticle synthesis (Al-Snafi, 2018; Vercruysse et al., 2024).

The objectives of this study were: (i) to recover and utilize the bioactive compounds from *Hedera helix* biomass; and (ii) to synthesize and characterize AuNPs from these bioactive compounds using a green, plant-mediated approach, and (iii) to evaluate the antioxidant and antimicrobial potential of both the extracts and the synthesized AuNPs.

MATERIALS AND METHODS

All utilized chemicals and reagents were of analytical grade and procured from Sigma-Aldrich and Merck.

Plant-based materials

Hedera helix L. leaves were gathered locally from Arad city, Romania (46°10′36″N 21°18′4″E). Until required, they were air-dried and then placed in paper bags for storage.

Preparing the plant extracts

The dry plant leaves were ground to a fine powder using an electric milling machine. Several extracts were prepared by 7 days aqueous maceration (HH1) and hydroalcoholic maceration (HH2) or a 30-minute aqueous infusion (HH3), using a 1:10 w/v plant biomass to solvent. The resulting extracts were filtered and further centrifuged at 8000 rpm for 15 minutes, and the upper layer was collected for AuNPs synthesis and biochemical analysis. For the UHPLC analysis, the extracts were filtered using a 15 mm, 0.45 μm PVDF syringe filter.

Biochemical Assays

Total Phenolic Content

Phenolic quantification was assessed using the Folin-Ciocalteu (FC) method, and the results were expressed as gallic acid equivalents (GAE/L) following the procedure described by Moisa et al. (2018). Briefly, diluted extract (1:25) was mixed and reacted with FC reagent, 20% sodium carbonate, and water, and the mixture was incubated for 90 minutes at room temperature in the dark. The absorbance values were read at a wavelength of 765 nm.

Antioxidant Activity

DPPH Assay

The DPPH• (1,1-diphenyl-2-picrylhydrazyl) free radical assay was performed following the method previously described by Csakvari et al. (2021). Briefly, 100 µL sample was mixed with 3 mL DPPH• solution and incubated in the dark for 1 hour. The absorbance was measured at 517 nm, and the results were expressed as a percentage of inhibition and mg GAE/L.

FRAP Assay (Ferric Reducing Antioxidant Power)

The antioxidant activity of the *Hedera helix* extracts was evaluated by measuring their ability to reduce the Fe^{3+}-TPTZ complex to its Fe^{2+}-TPTZ form, resulting in a blue-colored solution with a maximum absorbance at 593 nm. For this, FRAP reagent was freshly prepared by mixing acetate buffer (300 mM, pH 3.6), TPTZ solution (10 mM in 40 mM HCl), and $FeCl_3$ solution (20 mM) in a 10:1:1 (v/v/v) ratio, as described by Mot et al. (2022). For each assay, 0.2 mL of extract was mixed with 1.5 mL of FRAP reagent, incubated in the dark for 20 minutes, and the absorbance was recorded at 593 nm, using water as a blank.

Total Flavonoid Content

The previously obtained *Hedera helix* extracts were used to determine the flavonoid content following the method described by Copolovici et al. (2021). For this, 250 µL of the extract was mixed with 1250 µL of sodium acetate solution (100 g/L), 750 µL of aluminum chloride solution (25 g/L), and 250 µL of deionized water. The mixture was incubated in the dark for 15 minutes, and absorbance was measured at 434 nm against a reference sample prepared under the same conditions.

Statistical Analysis

Statistical analysis of the biochemical assay results was performed using two-way analysis of variance (ANOVA), followed by Tukey's multiple comparison test in order to determine significant differences between samples. Values presenting different superscript letters are significantly different ($p < 0.05$); values sharing the same letters are not significantly different ($p > 0.05$).

Chemical Composition Determined by UHPLC-DAD

The extracts were evaluated using an ultra-high-performance liquid chromatograph (UHPLC Nexera X2, Shimadzu, Tokyo, Japan) equipped with a reversed-phase Nucleosil C18 column (Macherey-Nagel, Düren, Germany), following the method described by Csakvari et al. (2021). Compounds were identified and quantified by comparing retention times and UV spectra with reference standards analysed under identical conditions.

Synthesis of Gold Nanoparticles

Gold nanoparticles were synthesized using a procedure adapted from Chiravoot et al. (2021), with several modifications. Therefore, 27 mL of 0.5, 1, and 2 mM $HAuCl_4 \cdot 3H_2O$ solution was added at 30 ˚C to 4 mL plant extract at room temperature under constant mixing. After 1 h of reaction time, the mixture was centrifuged at 8000 rpm for 30 minutes and then the supernatant was discarded. The resulting AuNPs were washed three times with deionized water and resuspended in a small volume to obtain a concentrated suspension, which was used for further analysis.

UV-Vis Characterization of AuNPs

UV–Vis spectroscopy analysis using a Specord 200 spectrophotometer (Analytik Jena AG, Germany), with the absorbance recorded in the range of 400–700 nm revealed a characteristic surface plasmon resonance (SPR) peak at

approximately 550 nm, confirming the presence of AuNPs.

SEM–EDS Characterization of AuNPs

The morphology, size, and distribution of the synthesized AuNPs from *Hedera helix* extracts were examined using a scanning electron microscope (SEM, LYRA 3 XMU, Tescan, Czech Republic) at 50 kx magnification. Elemental composition was assessed through Energy-Dispersive X-ray spectroscopy (EDS) (EDAX Inc., Mahwah, NJ, USA).

Antimicrobial Activity – MIC Assay

The antimicrobial potential of the concentrated AuNPs suspension was assessed through a broth microdilution method using a 96-well plate. The microbial strains used in this study (*E. coli* ATCC 25922, *S. typhimurium* ATCC 14028, *S. aureus* ATCC 25923, *C. albicans* ATCC 10231, *P. aeruginosa* ATCC 27853) were obtained from the in-house microbial collection of the "Aurel Vlaicu" University of Arad.

Following a microdilution protocol described by Hilpert et al. (2008), each well in columns 1 to 10 was initially filled with 100 µL of Mueller-Hinton Broth (MHB, VWR, BDH®). Afterward, a volume of 100 µL of the AuNPs stock suspension was added to the first well (column 1), mixed thoroughly, and 100 µL was transferred to the next well (column 2). This serial dilution continued until column 10, discarding the final 100 µL to maintain equal volumes.

Following the serial dilution, 100 µL of microbial inoculum adjusted to 0.5 McFarland standard (approximately 1.5×10^8 CFU/mL) was added to wells in columns 1 to 10. Column 11 was the positive control (200 µL of microbial inoculum in MHB), while column 12 was the negative control (200 µL of sterile MHB, without microorganisms).

Plates were incubated at 37 °C for 24 hours, and optical density (OD) was measured at two wavelengths, 600 nm and 620 nm, using a Tecan Spark multimode microplate reader (Tecan Group Ltd., Switzerland).

RESULTS AND DISCUSSIONS

Chemical Composition of the Hedera helix Extracts

All the extracts obtained were evaluated for their content of phenolic compounds and flavonoids, and their antioxidant activity was assessed.

The biochemical analyses indicated that the HH3 extract presented the highest total phenolic content (714.36 ± 63.48^a mg GAE/L), followed by the HH1 extract (515.13 ± 8.00^b mg GAE/L) and lastly, the HH2 extract (508.78 ± 8.18^b mg GAE/L), values sharing different superscript letters are significantly different ($p < 0.05$); values sharing the same letters are not.

The antioxidant activity measured using the DPPH method presented a comparable trend, with the HH3 extract showing a higher activity (58.76% inhibition; 28.45 ± 0.23 mg^a GAE/L), followed by the HH2 extract (43.74%; 20.46 ± 0.60^b mg GAE/L) and lastly the HH1 extract (17.96%; 6.74 ± 0.09^c mg GAE/L).

Flavonoid content and FRAP values were similar for all the extracts. For the flavonoid content, the results ranged from 0.24 ± 0.01^c meq rutin/mL in the HH1 extract to 0.32 ± 0.01^b and 0.38 ± 0.01^a meq rutin/mL in the HH3 and HH2 extracts, while for FRAP assay the results ranged from 0.52 ± 0.01^b to 0.55 mM $\pm 0.01^a$ Trolox/L.

Considering these results, only the infusion extract (HH3) was selected for nanoparticle synthesis due to its higher phenolic and antioxidant levels, quick preparation time, and avoidance of organic solvents.

Within the UHPLC analysis, several phenolic and antioxidant compounds in the *Hedera helix* extracts were confirmed (Figure 1). The highest concentration of rutin was observed in the HH3 extract (467.91 mg/L) and the HH2 extract (430.19 mg/L), while the HH1 extract contained the lowest amount (253.13 mg/L). Vanillic acid was also in a slightly higher concentration within the HH3 extract (299.61 mg/L), compared to the HH2 extract (281.58 mg/L), and was not detected in the HH1 extract. Caffeic acid followed a similar pattern, with 185.14 mg/L in HH3 and

44.06 mg/L in HH2, and was not detected in the HH1 samples.

However, ascorbic acid was only found in the macerates 90.65 mg/L in HH1 extract and 190.62 mg/L in the HH2 extract but was not detected in the HH3.

Table 1. UHPLC analysis of extracts

Compound mg/L	RT	HH1	HH2	HH3
Ascorbic acid	3.064	90.65	190.62	-
Vanillic acid	9.098	253.13	430.19	467.91
Rutin	9.397	-	281.58	299.61
Caffeic acid	9.676	-	44.06	185.14

These results are similar to those reported in existing literature for the extracts of *Hedera helix* leaves (Ahchouch et al., 2024; Shawky and El Sohafy, 2020).

The resulting data further support the biochemical assay results and justify the selection of the HH3 extract for nanoparticle synthesis due to its higher composition in phenolic compounds and the potential use of the reaction in the absence of organic solvents.

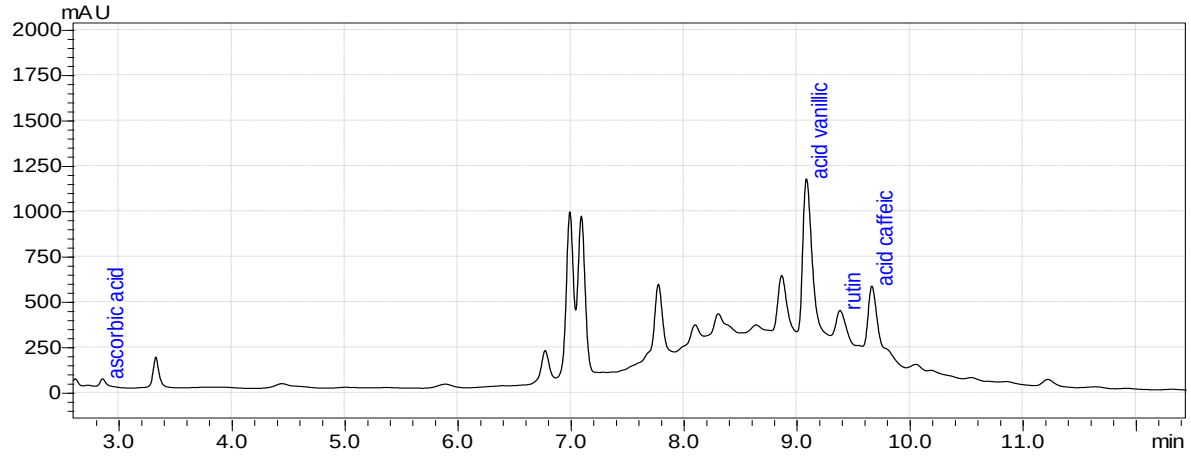

Figure 1. UHPLC chromatogram of *Hedera helix* extract

Synthesis and Optical Properties of AuNPs

The reaction between *HH3* extract and $HAuCl_4$ solutions revealed the synthesis of gold nanoparticles, which was visually observed by the color shift of the reaction mixtures from pale yellow to dark pink. UV corroborated the visual observation–Vis spectroscopy analysis, which presented distinctive surface plasmon resonance (SPR) peaks ranging from 540 to 550 nm (Figure 2) for all samples, as was also reported by Yi et al. (2013).

The intensity of the SPR peak increased with the concentrations of $HAuCl_4$ (0.5 mM < 1 mM < 2 mM), indicating a rapid nanoparticle synthesis. The higher intensity peak recorded for using the 2 mM gold solution could possibly indicate the development of a highly concentrated and perhaps monodisperse colloidal suspension.

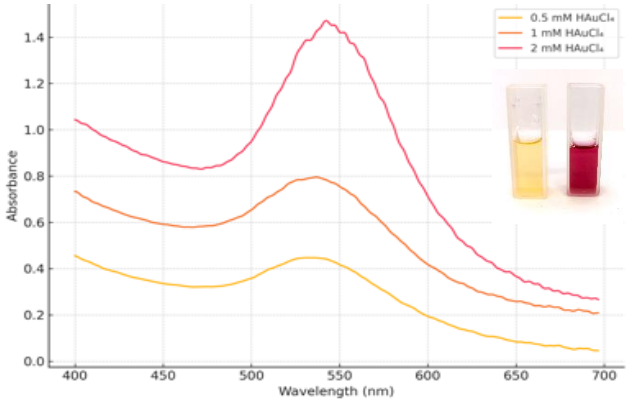

Figure 2. UV-Vis spectra after synthesis prior to purification of AuNPs.

The presence of a higher concentration of phenolic compounds, including rutin and caffeic acid, in the extract could have influenced the reduction and stability of the

nanoparticles, acting as reducing and capping agents.

AuNPs Morphological and Elemental Characterization

The biosynthesized AuNPs morphology was determined using a Scanning Electron Microscope (SEM) at 50 kx magnification for all samples. As depicted in Figure 3, the AuNPs synthesized from *HH3* extract and varying $HAuCl_4$ concentrations (0.5, 1, and 2 mM) presented predominantly spherical shapes, with an estimated diameter varying between 20 and 80 nm (Figure 3), with similar results reported by Xia et al. (2013).

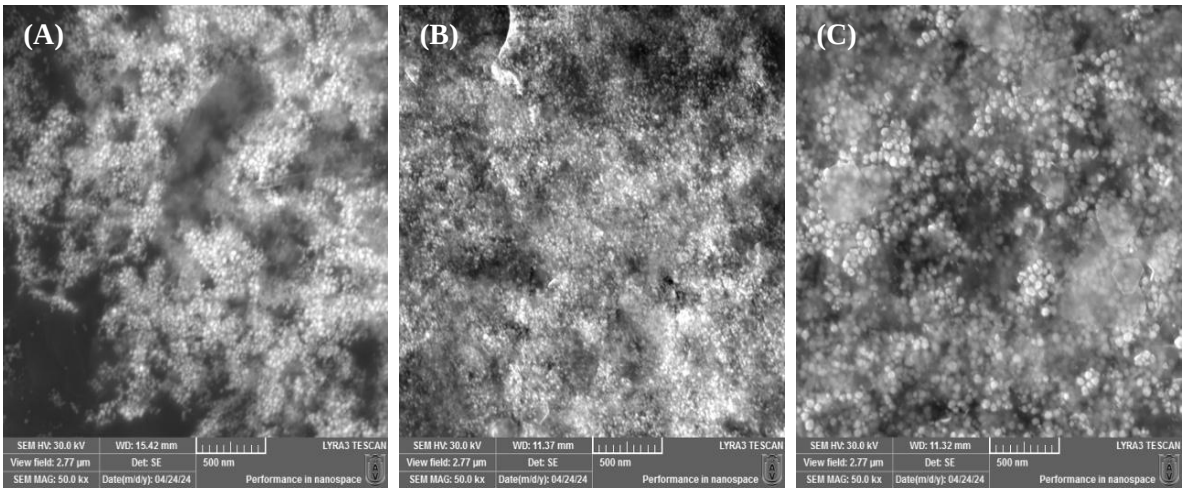

Figure 3. SEM micrographs of gold nanoparticles synthesized using HH3 extract and three different concentrations of $HAuCl_4$: (A) 0.5 mM, (B) 1 mM, and (C) 2 mM. All images were recorded at 50 kx magnification without prior sample coating.

More homogenous particle size and distribution were observed for the sample at 1 mM $HAuCl_4$, with reduced aggregation compared to 0.5 and 2 mM $HAuCl_4$ solution samples.

At the higher concentration (2 mM $HAuCl_4$), an increased particle density, clustering, and non-spherical structures were observed. These non-spherical structures presented truncated or irregular triangular shapes, suggesting a possible shift toward anisotropic growth specific for higher gold ion concentrations (Yi et al., 2013).

Therefore, due to their higher surface-to-volume ratio, which is characteristic of smaller and spherical nanoparticles, their ability to interact with microbial cell membranes, viruses and fungi, represents a crucial aspect for biomedical applications and the overall toxicity of metal NPs. (Osonga et al., 2020; Saed et al., 2024).

As was reported by Azad et al. (2023) morphological diversity can be caused by slight variation of the phytochemical composition of plant extracts and higher metal concentrations in the synthesis medium.

Energy Dispersive X-ray spectroscopy (EDS) analysis was used to determine the elemental composition of the biosynthesized AuNPs. In all samples, elemental gold (Au) was the main constituent, and strong distinctive peaks were observed at around 2.1 keV. Low-intensity signals were also detected and attributed to carbon (C), most probably from the small quantity of biomolecules from the extracts that may be present in the sample.

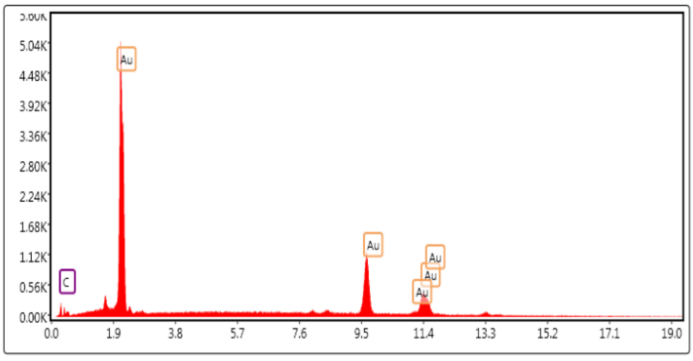

Figure 4. EDS spectrum of AuNPs synthesized using HH3 extract and 2 mM $HAuCl_4$.

As was presented in Figure 4, the gold content was overall high in all analyzed samples, with relative weight percentages of 87.9% (2 mM), 86.7% (0.5 mM), and 78.5% (1 mM), further supporting the successful biosynthesis of AuNPs using HH3 extract.

These results validate the efficiency of the green synthesis method and correlate with the SEM observations of nanoparticle size and distribution.

Antimicrobial Activity of AuNPs

Microbiological analyses were performed using the broth microdilution method to determine the antimicrobial potential of *Hedera helix*-derived gold nanoparticles biosynthesized at three different synthesis medium concentrations (0.5, 1, and 2 mM $HAuCl_4$) alongside two standard antibiotics. Fresh microbial cultures were prepared, and prior to inoculation, they were adjusted to 0.5 McFarland, and afterward, they were inoculated in 96-well microplates containing serial dilutions of the AuNPs suspensions.

The resulting BIR% values are indicating that the *Hedera helix*-mediated biosynthesized AuNPs did not exhibit inhibitory effects against the five tested microbial strains under the conditions employed. However, these results were affected due to substantial optical interference caused by the AuNPs. In contrast, both reference antibiotics demonstrated strong antimicrobial activity. A limitation of this study is the absence of an antifungal agent as a control and an antimicrobial protocol optimization is required. These findings also suggest that further adjustment of the synthesis protocol is required, either to enhance nanoparticle dispersion efficiency or to functionalize their surface with bioactive ligands, thereby improving the antimicrobial efficacy of the green-synthesized AuNPs.

CONCLUSIONS

The extracts obtained from *Hedera helix* biomass were characterized and presented remarkable antioxidant potential and moderate content of phenolic and flavonoid compounds. It represents a good source of bioactive compounds that can be successfully used to biosynthesize gold nanoparticles (AuNPs) of both spherical and polydisperse shapes, as confirmed by UV–Vis and SEM-EDS analyses, representing a sustainable approach for the valorization of plant-based biomass found in high amount in vertical greenery systems present in city landscapes.

However, the MIC antimicrobial assay against several microbial strains (bacteria and fungi) revealed that the biosynthesized nanoparticles presented low antimicrobial activity compared to standard antibiotics. These results suggest that, although AuNP synthesis was effective, further optimization of either the particle surface or their concentration is still necessary for enhancing antimicrobial properties, therefore, AuNPs with low antimicrobial activity could be functionalized and used as drug delivery carriers to enhance their antimicrobial potential.

ACKNOWLEDGEMENTS

This work was supported by a grant of the Ministry of Research, Innovation and Digitization, CNCS - UEFISCDI, project number PN-III-P4-PCE-2021-0639, within PNCDI III and by a grant from the Romanian Ministry of Education and Research, CNCS—UEFISCDI, project number PN-III-P1-1.1-PD-2019-0607, within PNCDI III.

REFERENCES

Ahchouch, H., El house, M., Al-Moubaraki, A.H., Noor, E.A., Hadfi, A., Driouiche, A., Bammou, L., Belkhaouda, M.h., Salghi, R., Chafiq, M., Chaouiki, A., Ko, Y.G., 2024. From nature to protection: Unleashing the protective potential of Hedera helix leaves against corrosion in harsh acidic environments using experimental and theoretical insights. Arabian Journal of Chemistry 17, 105593.

Al-Snafi, A., 2018. Pharmacological and therapeutic activities of Hedera helix-A review. 8.

Azad, A., Zafar, H., Raza, F., Sulaiman, M., 2023. Factors Influencing the Green Synthesis of Metallic Nanoparticles Using Plant Extracts: A Comprehensive Review. pharmafronts 05, 117-131.

Baharara, H., Moghadam, A.T., Sahebkar, A., Emami, S.A., Tayebi, T., Mohammadpour, A.H., 2021. The Effects of Ivy (Hedera helix) on Respiratory Problems and Cough in Humans: A Review. Adv Exp Med Biol 1328, 361-376.

Belete, T.M., 2019. Novel targets to develop new antibacterial agents and novel alternatives to antibacterial agents. Human Microbiome Journal 11, 100052.

Belmehdi, O., Taha, D., Abrini, J., Ming, L.C., Khalid, A., Abdalla, A.N., Algarni, A.S., Hermansyah, A., Bouyahya, A., 2023. Anticancer properties and mechanism insights of α-hederin. Biomedicine & Pharmacotherapy 165, 115205.

Bezruk, I., Marksa, M., Georgiyants, V., Ivanauskas, L., Raudone, L., 2020. Phytogeographical profiling of ivy leaf (Hedera helix L.). Industrial Crops and Products 154, 112713.

Copolovici, L., Lupitu, A., Moisa, C., Taschina, M., Copolovici, D.M., 2021. The Effect of Antagonist Abiotic Stress on Bioactive Compounds from Basil (Ocimum basilicum). Applied Sciences 11, 9282.

Csakvari, A.C., Moisa, C., Radu, D.G., Olariu, L.M., Lupitu, A.I., Panda, A.O., Pop, G., Chambre, D., Socoliuc, V., Copolovici, L., Copolovici, D.M., 2021. Green Synthesis, Characterization, and Antibacterial Properties of Silver Nanoparticles Obtained by Using Diverse Varieties of Cannabis sativa Leaf Extracts. Molecules 26, 4041.

Gavrila, A.I., Zalaru, C.M., Tatia, R., Seciu-Grama, A.M., Negrea, C.L., Calinescu, I., Chipurici, P., Trifan, A., Popa, I., 2023. Green Extraction Techniques of Phytochemicals from Hedera helix L. and In Vitro Characterization of the Extracts. Plants (Basel) 12.

Moisa, C., Copolovici, L., Bungau, S., Pop, G., Imbrea, I., Lupitu, A., Nemeth, S., Copolovici, D., 2018. Wastes resulting from aromatic plants distillation - bio-sources of antioxidants and phenolic compounds with biological active principles. Farmacia 66, 289-295.

Mot, S.E.L., Salajan, P.A., Moisa, C., Copolovici, L., Copolovici, D.M., 2022. Chemical and Antioxidant Capacity Evaluation of *Centaurea jacea* Extracts from Plants Harvested in Arad County, Romania. Scientific and Technical Bulletin, Series: Chemistry, Food Science and Engineering 19, 53-62.

Mungwari, C.P., King'ondu, C.K., Sigauke, P., Obadele, B.A., 2025. Conventional and modern techniques for bioactive compounds recovery from plants: Review. Scientific African 27, e02509.

Osonga, F.J., Akgul, A., Yazgan, I., Akgul, A., Eshun, G.B., Sakhaee, L., Sadik, O.A., 2020. Size and Shape-Dependent Antimicrobial Activities of Silver and Gold Nanoparticles: A Model Study as Potential Fungicides. Molecules 25, 2682.

Pechyen, C., Ponsanti, K., Tangnorawich, B., Ngernyuang, N., 2021. Waste fruit peel – Mediated green synthesis of biocompatible gold nanoparticles. Journal of Materials Research and Technology 14, 2982-2991.

Rónavári, A., Igaz, N., Adamecz, D.I., Szerencsés, B., Molnar, C., Kónya, Z., Pfeiffer, I., Kiricsi, M., 2021. Green Silver and Gold Nanoparticles: Biological Synthesis Approaches and Potentials for Biomedical Applications. Molecules 26, 844.

Saed, M., Ayivi, R.D., Wei, J., Obare, S.O., 2024. Gold nanoparticles antibacterial activity: Does the surface matter? Colloid and Interface Science Communications 62, 100804.

Saravanan, M., Barabadi, H., Vahidi, H., 2021. Chapter 5 - Green nanotechnology: isolation of bioactive molecules and modified approach of biosynthesis, in: Patra, C., Ahmad, I., Ayaz, M., Khalil, A.T., Mukherjee, S., Ovais, M. (Eds.), Biogenic Nanoparticles for Cancer Theranostics. Elsevier, pp 101-122.

Sen, N.B., Guzelmeric, E., Vovk, I., Glavnik, V., Kırmızıbekmez, H., Yesilada, E., 2023. Phytochemical and Bioactivity Studies on Hedera helix L. (Ivy) Flower Pollen and Ivy Bee Pollen. Antioxidants 12, 1394.

Shawky, E., El Sohafy, S.M., 2020. Untargeted and targeted chemical profiling for efficacy-directed discrimination of Hedera helix L. subspecies using HPTLC- image analysis and HPTLC/MS. Industrial Crops and Products 145, 111980.

Shokry, A.A., El-Shiekh, R.A., Kamel, G., Bakr, A.F., Ramadan, A., 2022. Bioactive phenolics fraction of Hedera helix L. (Common Ivy Leaf) standardized extract ameliorates LPS-induced acute lung injury in the mouse model through the inhibition of proinflammatory cytokines and oxidative stress. Heliyon 8, e09477.

Sorbiun, M., Shayegan Mehr, E., Ramazani, A., Mashhadi Malekzadeh, A., 2018. Biosynthesis of metallic nanoparticles using plant extracts and evaluation of their antibacterial properties. Nanochemistry Research 3, 1-16.

Suica-Bunghez, I.-R., Ana-Alexandra, S., Doncea, S., Constantin, M., Raut, I., Ion, R.-M., 2020. Phytochemical, antioxidant and antimicrobial characterization of *Hedera helix* L. extract. Journal of Plant Development 27, 47-53.

Thipe, V.C., Karikachery, A.R., Çakılkaya, P., Farooq, U., Genedy, H.H., Kaeokhamloed, N., Phan, D.-H., Rezwan, R., Tezcan, G., Roger, E., Katti, K.V., 2022. Green nanotechnology—An innovative pathway towards biocompatible and medically relevant gold nanoparticles. Journal of Drug Delivery Science and Technology 70, 103256.

Vaou, N., Stavropoulou, E., Voidarou, C., Tsigalou, C., Bezirtzoglou, E., 2021. Towards

Advances in Medicinal Plant Antimicrobial Activity: A Review Study on Challenges and Future Perspectives. Microorganisms 9, 2041.
Vercruysse, W., Kunnen, K., Gomes, C.L., Marchal, W., Cuypers, A., Vandamme, D., 2024. Common Ivy (Hedera helix L.) Derived Biochar's Potential as a Substrate Amendment: Effects of Leached Nutrients on Arabidopsis thaliana Plant Development. Waste and Biomass Valorization 15, 2071-2082.
Wiegand, I., Hilpert, K., Hancock, R.E.W., 2008. Agar and broth dilution methods to determine the minimal inhibitory concentration (MIC) of antimicrobial substances. Nature Protocols 3, 163-175.
Wyka, J., Piechnik, Ł., Grzędzicka, E., Lešo, P., Dyderski, M.K., Kajtoch, Ł., 2023. The vertical form of the common ivy Hedera helix L. is associated with diverse and semi-natural forests in Central European highlands. Forest Ecology and Management 530, 120750.
Yi, S., Xia, L., Lenaghan, S.C., Sun, L., Huang, Y., Burris, J.N., Stewart, C.N., Jr., Zhang, M., 2013. Bio-synthesis of gold nanoparticles using English ivy (Hedera helix). J Nanosci Nanotechnol 13, 1649-1659.

ISSN 1582-1021
e-ISSN 2668-4764
Edited by "Aurel Vlaicu" University of Arad Publishing House, Arad, Romania

10.62591/Scien.Tech.Bull-Chem.FoodSci.Eng.2024.21.04

Review

LATEST PROGRESS ON LUMINESCENT HOMO- AND HETERO-POLYMETALLIC METALLOMESOGENS BASED ON *d*-BLOCK METAL COMPLEXES

Evelyn POPA, Elisabeta I. SZERB, Carmen CRETU*

"Coriolan Dragulescu" Institute of Chemistry, Romanian Academy
24 Mihai Viteazu Bvd., 300223 Timisoara, Romania
Corresponding author email: cretucarmen@acad-icht.tm.edu.ro

Abstract: *Luminescent liquid crystalline metal complexes are attractive multifunctional materials due to their great potential of applicability in a wide range of domains from technological to medical fields. This review is focused on the luminescent homo– and hetero–polymetallic metallomesogens containing d-block metal ions and different mono and polydentate ligands published in the last ten years highlighting their ability to self-assembly in ordered lamellar or columnar phases according to their molecular structure. The luminescent properties in solution, solid and liquid crystalline states are also discussed.*

Keywords: polymetallic metallomesogens, *d*-block metal complexes, luminescent properties.

INTRODUCTION

Liquid crystals are considered promising materials for different applicative fields due to their adaptive and controllable stimulus responsiveness characteristics with numerous applications beyond liquid crystal displays (LCDs) (Bisoyi et al. 2022). Despite the great potential in various technological, scientific and medical fields, there is a constant need to improve their properties to increase performance in the field of interest. Luminescent liquid crystals are considered novel materials in the production of energy-efficient display devices through their ability to enhance colour, brightness and view angle of display dispositive, eliminating dependency of LCDs by other expensive brightness sources (Kumar et al. 2023). The introduction of a metallic centre into liquid crystals, called "metallomesogens", gives them unique and desirable properties compared to organic liquid crystals: electrical, redox, magnetic, optical, etc., properties induced by the metal ion (Giménez et al. 2002), being considered extremely promising materials for application in optoelectronics (Krikorian et al. 2014, Geng et al. 2017, Wang et al. 2016), energy (Ionescu et al. 2012, Su et al. 2016), medicine and even in agriculture (Hakemi et al. 2022). The presence of a second metal ion in the molecular architecture can tune the target properties of the final homo or hetero-bimetallic complex. Moreover, hetero-bimetallic species (metal complexes containing two different metal centre) bring additionally physicochemical properties, metallic complementarity and/or synergism, increasing the capacity for novel application (Wenzel et al. 2014). In the literature, are known some examples of homo- (Cuerva et al. 2021) and hetero-polymetallic metallomesogens (Kadkin et al. 2008) obtained by direct metal-ligand synthesis without an accurate analysis of their functionality-related characteristics. To date, most of luminescent metallomesogens reported are monometallic, and their optical behaviour was studied in solid state or solution (Wang et al. 2012, Wu et al. 2018, Santoro et al. 2009). Due to their reduced stability and high transition temperatures, the optical measurements in the liquid crystalline states become problematic. However, through a proper and smart design of such materials, these drawbacks can be solved obtaining liquid crystals at relatively low to room temperature. Thus, only a limited example of liquid crystalline metal complexes based on zinc(II), copper(I), gold(I), silver(I) and lanthanide(III) ions have shown luminescent properties in liquid crystalline state (Szerb et al. 2022, Binnemans et al. 2009).

Herein, we present the recent progress over the last decade in development of luminescent

metallomesogens containing more than one *d*-block metal centre.

CLASIFICATION OF LUMINESCENT POLYMETALLIC METALLOMESOGENS

Homo–polymetallic metallomesogens

This kind of compounds are liquid crystalline metal complexes that contain two or more identical metal ions coordinated to mono/polydentate ligands forming metal oxide/halogen/fluorophenyl bridged complexes, metallacycles, metallacages, etc.

Chico et al. 2016 reported a homo–bimetallic linear Au(I) complex (**1**) based on a mesogenic isocyanide triphenylene ligand and a biphenytetrafluoro-linker (Figure 1a). The complex displayed polymorphism when compared to its free ligand that showed only a columnar hexagonal mesophase (Colh) (Figure 1b) from 37 to 130 ºC. Thus, complex **1** organized at high temperatures into nematic phase (N) between 122 and 172 ºC and at lower temperatures exhibited columnar rectangular (Colr) from 102 to 122 ºC.

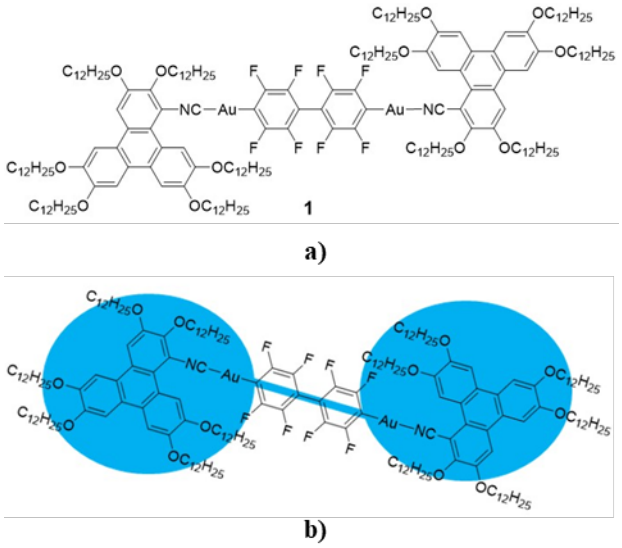

Figure 1. Chemical structure of **1** (a); The proposed molecular packing of **1** (b).

The Au(I) complex **1** showed a blue-violet emission (λex = 282 nm, λem = 420 nm,) in solution (CH_2Cl_2, 10^{-5}M) at room temperature, similar with the free ligand. However, the emission quantum yield of the complex [Φ (x10^{-3}) = 0.0028] was significantly reduced when compared to the ligand [Φ (x10^{-3}) = 0.2800] due to the increasing of the non-radiative deactivation process generated by the heavy metal effect (Ibrayev et al. 2024). The luminescence of **1** is quenched at higher concentration and also in the solid state and mesophase. Other linear type of bimetallic complexes reported (Al-Karawi et al. 2017) (**2**–**4**) (Figure 2a) contain hydrazine-based mesogenic ligands that exhibited nematic phases. Their Ag(I) complexes organized into smectic phases at relatively low temperatures (Table 1).

Table 1. DSC and emission data for Ag(I) complexes **2**–**4**

Comp.	Phase transitions T_{max}°C (ΔH/KJ.mol^{-1}) first heating/cooling	Emission data on solid and mesomorphic state, λem/nm (λex = 248 nm)
2	Cr_1–Cr_2 84.2 (20.21) Sm 125.1 (18.67) I / I 123.3 (−19.40) Sm 73.4 (−22.61) Cr_2–Cr_1	494
3	Cr_1–Cr_2 79.5 (23.31) Sm 113.4 (19.44) I / I 108.2 (−20.94) Sm 65.9 (−24.82) Cr_2–Cr_1	494
4	Cr_1–Cr_2 83.1 (21.24) Sm 115.3 (18.81) I / I 112.7 (−19.60) Sm 68.3 (−23.20) Cr_2–Cr_1	493

Cr - crystalline solid, Sm - smectic mesophase, I - isotropic liquid

For these bimetallic silver(I) complexes, some interesting characteristics governed the liquid crystalline properties. In particular, similar bimetallic silver(I) complexes with shorter (n < 6) or longer chain lengths (n > 8) or with an asymmetric position of the azine group (not shown herein) were not mesomorphic. The liquid crystalline Ag(I) complexes (**2**–**4**) revealed intense blue emission at room temperature, both in solid and mesomorphic state (Table 1) attributed to a ligand-centred transition. However, in the isotropic phase, the luminescence was totally quenched but upon cooling it returns (Figure 2b).

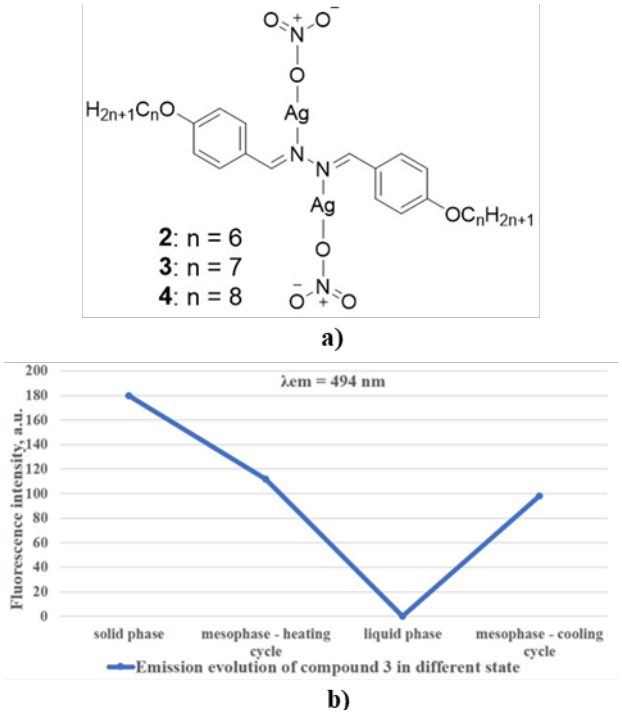

Figure 2. Chemical structure of Ag(I) metallomesogens (a); fluorescence evolution of complex **3** in solid, mesomorphic and liquid phase (b).

Micutz et al. 2014 obtained two homo-bimetallic Pd(II) complexes (**5** and **6** – Figure 3a) based on a Schiff base and an ancillary benzoyl-thiourea ligands showing mesomorphic properties at low temperatures. Their strategy to obtain room temperature metallomesogens was to vary the number of alkyl chains grafted on the ancillary ligands. Both complexes self-assembled into disordered columnar hexagonal phases that formed glassy mesophases at room temperature. The organization inside the columns slightly differ in the case of the two metal complexes, in the number of molecules filling the disks, from approximatively two molecules for **5** to one molecule for **6** (Figure 3b).

The complexes were emissive in solid state, solution and in the mesophase at room temperature showing a red emission attributed to an intra-ligand transition (Table 2).

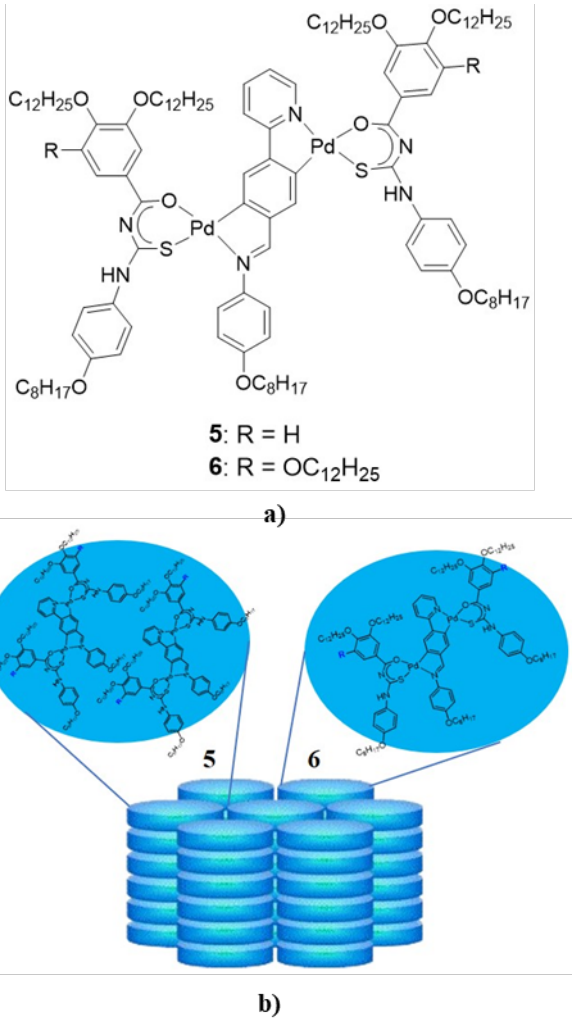

Figure 3. Chemical structure of metallomesogens **5** and **6** (a); the number of molecules that form columnar hexagonal unit (b).

Table 2. Emission data of binuclear Pd(II) complexes **5** and **6**

Comp.	Emission, λem/nm (Φ/%)		
	Solid state (λex = 480 nm)	Solution (CH_2Cl_2), $C_M = 5 \times 10^{-4}$ (λex = 283 nm)	Condensed state at room temperature
5	546, 676, 736, 819(sh)	365(0.55)	Similar to solid state
6	556, 683, 744, 823(sh)	360(0.39)	Similar to solid state

Pastor et al. 2018 published a series of metal complexes based on derivatives of pyridyl-β-diketone ligands differently substituted with alkyl chains where the position of N-pyridine atom dictated the type of complexes obtained and the liquid crystalline properties in the resulting compounds. Hence, the bimetallic complexes (dimers) **7**–**10** were obtained with the ligands containing the pyridyl nitrogen atom placed in *ortho* position, where the zinc(II) atoms were linked by two bridging chlorine

atoms (Figure 4a), while the ligands with *para* position of the nitrogen atom have led to mononuclear Zn(II) complexes. These complexes showed SmA phases at high temperatures (over 180 ºC) in a very short range of temperature (3 to 6 ºC) followed by a re-entrant crystal phase on heating cycle until the clearing temperature (Figure 4b). On cooling cycle, the complexes froze in SmA phase.

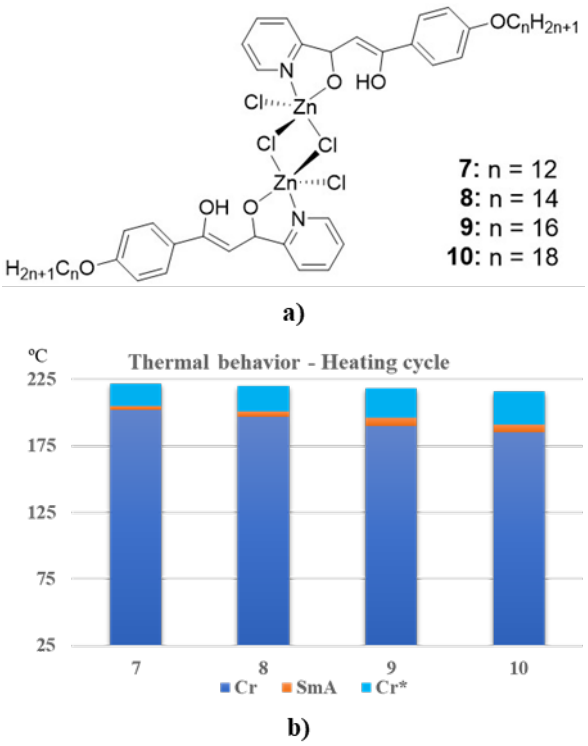

Figure 4. Chemical structure of metallomesogens **7**–**10** (a); thermal behaviour of the complexes (b) on heating cycle.

Nevertheless, these dimeric complexes had solubility problems that did not allowed the study of the luminescent properties in solution. However, the photophysical behaviour in solid state of only compound **7** was reported as representative of this class showing a blue emission (λem = 495 nm).

Pyridine-pyrazolate derivative ligands seem to have an interesting influence on the organization pattern of their Ag(I) complexes depending on the solvent polarity (Soria et al. 2016). Thus, in polar media, 1D oligomers are formed and in apolar solvents cyclic trimers are isolated, the last arrangement being predominantly encountered (Titov et al. 2019, Fujisawa et al. 2021). Therefore, three luminescent homo-polymetallic Ag(I) metallomesogens (**11**–**13**) based on pyridine-pyrazolate type ligands, with cyclic structure and different alkyl chain length were reported by Soria et al. 2016 (Figure 5a). The complexes presented a trimeric structure in solid state that become an open chain 1D oligomeric structure in mesomorphic state and in solution, the Ag-N bond proving to be too weak to maintain the cyclic structure. These 1D oligomeric forms allowed them to self-assembly in smectic A phases at relatively high temperature, over 100 ºC, and for compounds **12** and **13** the isotropization point (over 170 ºC) was accompanied by decomposition.

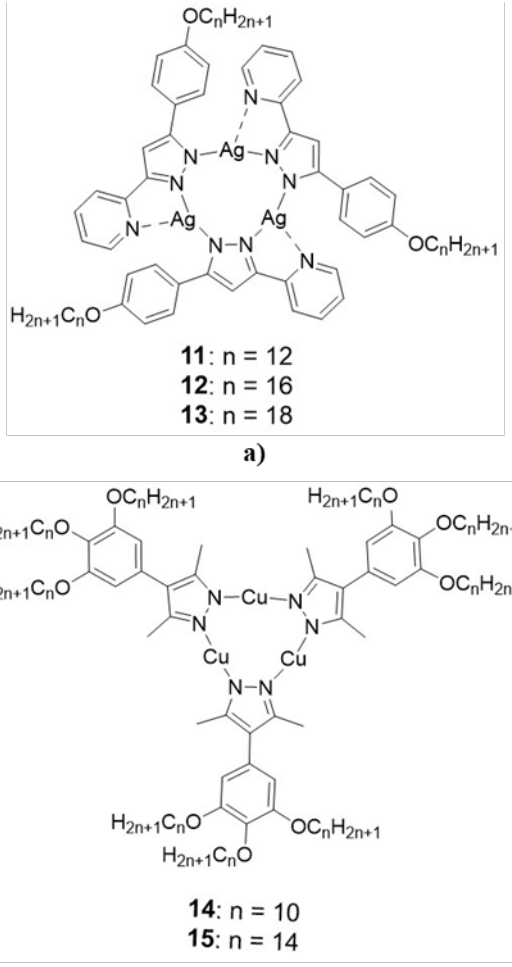

Figure 5. Chemical structure of metallomesogens **11**–**13** (a) and **14** and **15** (b).

All the Ag(I) complexes (**11**–**13**) emit in solution (λem = 386 nm, Φ = 0.07 for **11**) in their oligomeric form and become non-emissive in the cyclic form. Other cyclic homo–trimetallic Cu(I) metallomesogens (**14** and **15**) (Figure 5b) derived from phenyl-pyrazolinic ligands with phosphorescent properties were lately reported by Gimenez et al. 2020. Unlike the Ag(I)

metallomesogens **11**–**13**, the Cu(I) complexes displayed stable 2D columnar hexagonal (Colh) phases over a large temperatures range (108 ºC and 57 ºC, respectively) and lower clearing temperatures. On cooling cycle, both complexes froze in the mesophase at room temperature. The emissive properties were recorded on neat thin films at room temperature in Colh phase for **14** and in the crystalline phase and mesomorphic state, respectively (50 ºC) for **15**. In all cases, an orange–red light emission (661–664 nm) was observed due to the metal-centred triplet state (^{3}MM) excimer transition with an impressive quantum yield value of 42% for **14**. By increasing temperature from room temperature to 50 ºC for **15** a reducing of emission intensity and a minor decrease of lifetime (from 26 to 22 microseconds) were reported. In diluted THF solution, the complexes had a different behaviour showing a violet light emission similar with mesogenic phenyl-pyrazoles type ligands (Blanco et al. 2016). Huitorel et al. 2016 obtained an interesting dual emissive Cu(I) metallomesogen (**16**) based on a [Cu_4I_4] cubane cluster and phosphine-based ligands containing cyanobiphenyl (CBP) as mesogenic moieties (Figure 6a). The Cu(I) cluster (**16**) exhibited a smectic A mesophase over a wide range of temperature from 25 ºC to 100 ºC where the organic moieties (ligand) alternate with the inorganic ones ([Cu_4I_4] core) (Figure 6b).

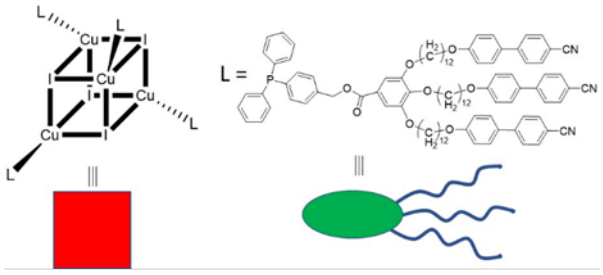

Figure 6. Chemical structure of metallomesogen **16** (a); schematic representation of proposed self-assembly of **16** into smectic A phase (b).

Under the UV light, the complex **16** showed a blue emission at room temperature that become greener by decreasing temperature to -196 ºC. This temperature-luminescence dependency is known as thermochromism. Moreover, the luminescence was also influenced by mechanical stimuli as grinding/crushing that generated changes at molecular level by shortening the metallophilic copper-copper bonds and altering the ligands organization. Thus, considerable changes in the colour emission from blue to green-yellow were observed. Chen et al. 2020 reported a luminescent rhomboidal metallacycle (**17**) with both thermotropic and lyotropic properties, formed through a donor-acceptor interaction between an organic donor such as tetraphenylethene moiety and a bimetallic Pt(II) complex bearing hydrophilic chains as acceptor unit (Figure 7).

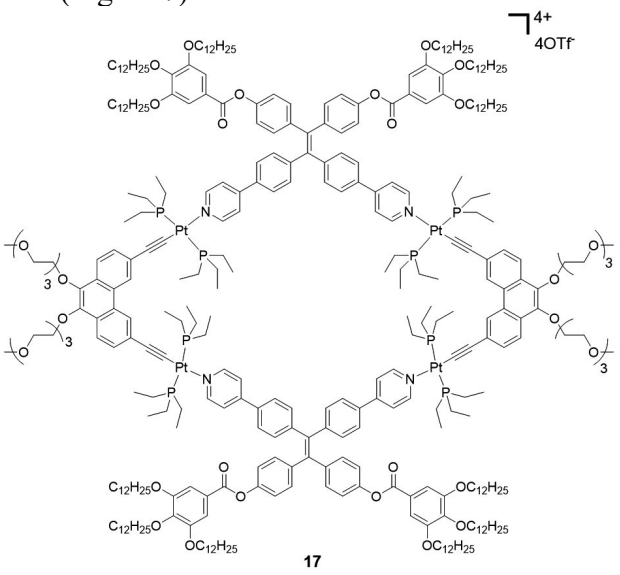

Figure 7. Chemical structure of metallomesogen **17**

The metallacycle **17** self-assembled into a 2D Colr phase at room temperature, stable up to 110 ºC, while in DMF solution organizes into Colh mesophase. Through irradiation with UV light (λex = 365 nm) in solution of dichloromethane, the complex **17** emitted green light (544 nm). In dichloromethane/hexane mixture, a progressively increased emission intensity was observed when hexane was gradually added. The increase of the luminescence was attributed

to aggregate formation. The intensity of emission become significant when the hexane volume fraction exceeds 60% recording an increase of the quantum yield value from 1.12% to 8.37%. In the liquid crystalline state, the value of the quantum yield was higher (12.6%) compared to the solution at room temperature with increasing temperature. Furthermore, the influence of temperature on the emission of **17** in the liquid crystalline phase revealed the expected decreasing of the intensity emission due to increase of vibrational modes. So, all these evidences revealed the AIE characteristics of this homo–polymetallic metallacycle.

Hetero–polymetallic metallomesogens

The need of designing hetero–polymetallic metallomesogens with synergistic properties is imperative in the development of more sophisticated and smart devices. In the last few years, there has been a stagnation in the publication of luminescent metallomesogens that contain different metal ions since obtaining these compounds is a real challenge from a synthetic point of view. In this regard, our team reported two luminescent hetero–polymetallic (**18**) and (**19**) metallomesogens obtained from terpyridine derivative ligand and substituted gallate co-ligands bearing ferrocene units (Fc) (Andelescu et al. 2024) (Figure 8).

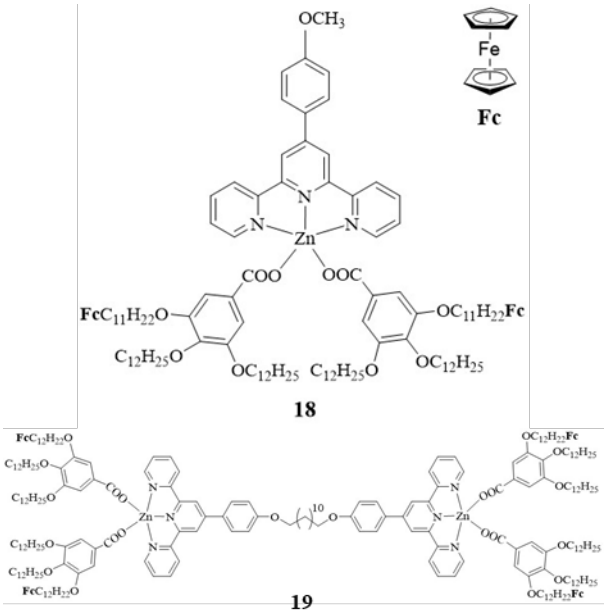

Figure 8. Chemical structure of metallomesogens **18** and **19.**

Both metal complexes exhibited 2D columnar hexagonal mesophases at room temperature for **18** and close to room temperature for **19** (70 ºC) stable up to 188 ºC and 156 ºC, respectively. The presence of the aliphatic chain that linked the two Zn units (**19**) decreased the izotropization temperature to 156 ºC for this complex. Moreover, the presence of the ferrocene fragment inserted into the aliphatic region of these metallomesogens leaded to a lower degree of the mesophase order, from 3D Mhex in the monometallic Zn(II) analogues (Popa et al. 2023) to 2D Colh in the polymetallic species (Popa et al. 2023). The photophysical properties of these metallomesogens were studied in solution and in the condensate states. Thus, in dichloromethane solution a violet emission (414 nm for **18** and 428 nm for **19**) was observed the red-shift of the emission maxima of complex **19** was attributed to vibrational motions caused by the bridging alkyl chain that link the two zinc containing units in case of **19**. The influence of the ferrocene unit in these hetero–polymetallic metallomesogens was also reflected through a red shift of the emission maxima in solution of both discussed compounds compared to their parent monometallic Zn(II) metallomesogen without ferrocene units (405 nm). Furthermore, by using different polarity solvents from polar (DMSO) to apolar ones (hexane) or increasing the polarity by gradually adding methanol to a dichloromethane solution containing the complex, significant changes in the photophysical properties were observed. Thus, by increasing the polarity of the media, an enhancement of the intensity and a red-shift of emission maxima was observed. Unfortunately, in the liquid crystalline state the emission was totally quenched when it was recorded at an excitation wavelength of 490 and 580 nm which correspond to the absorption of the molecule forming the Colh arrangement. However, a weak emission band centred at 430 nm was observed when excited at λex = 350 nm emission attributed to the single non-aggregated molecules.

Other strategy to obtain hetero–bimetallic metallomesogens was by simply chemical blending of Cu(II) and Zn(II) metallomesogens that are structurally-related (Cretu et al. 2023). Both metal complexes are hexacoordinated with

an identical coordination sphere formed by the chelation of one 1,10-phenanthroline ligand and two functionalized gallate co-ligands (Figure 9a).

Even though the monometallic complexes (Zn_MM and Cu_MM) were structurally similar, the Zn(II) complex formed Colr mesophase while the Cu(II) complex self-organized into Colh mesophase, their isotropization temperature being around 100 ºC. By mixing these two monometallic complexes in three different mass ratio (1:3, 1:1 and 3:1), three chemical blends (**20**: ZnCu = 1:3, **21**: ZnCu = 1:1 and **22**: ZnCu = 3:1) were obtained.

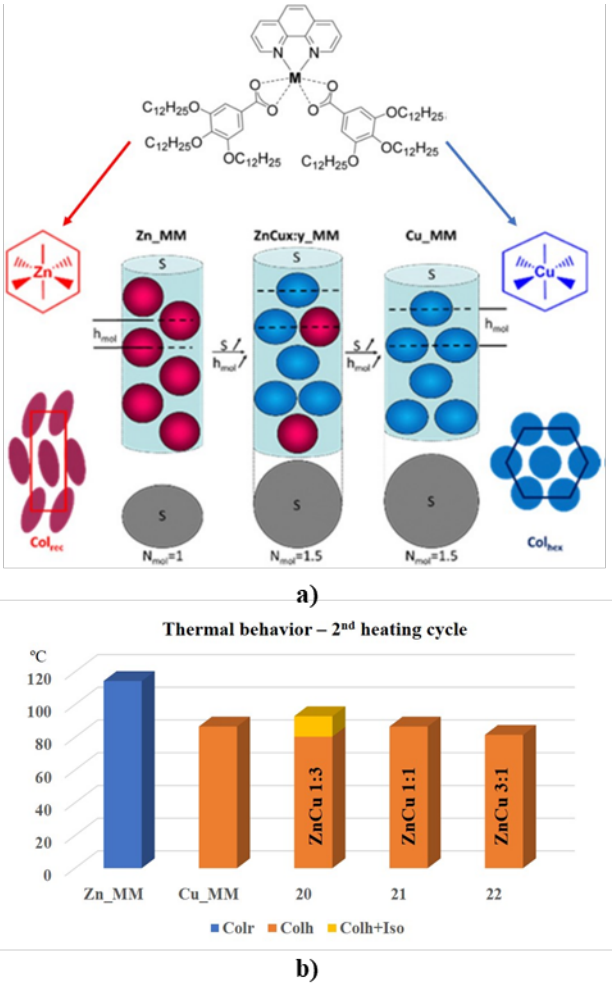

Figure 9. Schematic representation of the proposed self-assembly of the metallomesogenic precursors and the blends (a); thermal behavior of the blends **20–22** and their precursor (b)

From the mesomorphic point of view, all the blends self-assembled into Colh phases. The presence of the Cu(II) complex in these blends seem to stabilize the mesophase with higher symmetry (Colh). Small differences in the clearing temperature were observed, especially in case of blend **20** that contained a mixture of Colh and isotropic liquid before isotropization (Figure 9b). The photophysical properties of the blends were recorded in the condensed phases, and only the blend **20** was emissive in mesophase with an emission maximum centered at 520 nm (λex = 350 nm) and a lifetime value of 4.9 ns. The emission of **20** was similar to that of monometallic Zn_MM precursor in the mesophase, while in case of **21** and **22**, the non-emissive behaviour was attributed to the quenching effect of Cu_MM. Moreover, a small shoulder having the maximum at 445 nm was observed in the emission spectra of blend **20**, assigned to Cu_MM precursor emission. Despite the quenching of the emission properties in this case, this strategy of obtaining bimetallic liquid crystalline systems by chemical blending may shows potential due to the straightforward synthesis compared to the classical ones.

CONCLUSIONS

In this short review, we outlined the homo– and hetero–polymetallic luminescent liquid crystals progress recorded in the last decade involving different mono and polydentate ligands and different metal centres such Ag(I), Au(I), Cu(I), Pd(II), Pt(II), Zn(II) and Cu(II). Thus, mesogenic or non-mesogenic ligands based on isocyanide, hydrazine, imine, thiourea, halo, phosphine, pyridyl, pyrazoles and carboxylate derivatives were used to synthesize polymetallic liquid crystalline metal complexes. Their mesomorphic properties are influenced by a series of factors as the length, number and position of alkyl chains, the position of the donor atoms involved in the metal ion coordination that controls the type of the resulting metal complex, the molecules' symmetry and shape, etc. To design luminescent metallomesogens, some additional aspects has to be considered starting from choosing appropriate metal ions that can induce emission in the resulting metal complex or using highly conjugated organic ligands with optical properties. The emission properties of these systems are highly influenced by the polarity of the solution or molecular environment and the aggregation phenomena. Additionally, metallophilic interactions can be formed with specific transition metal ions like Cu(I), Ag(I),

Au(I) or Pt(II), playing an important role in tuning or altering the emission properties.

ACKNOWLEDGEMENTS

We acknowledge the Romanian Academy of Science (Program 4, Project 4.1.) for support.

REFERENCES

Al-Karawi, A.J.M., 2017. From Mesogens To Metallomesogens. Synthesis, Characterisation, Liquid Crystal And Luminescent Properties. Liq. Cryst. 44(1), 1-15, http://dx.doi.org/10.1080/02678292.2017.1371799.

Andelescu, A.A., Candreva, A., Popa, E., Visan, A., Cretu, C., La Deda, M., Szerb, E.I., 2024. Role of the Environment polarity on the Photophysical Properties of Mesogenic Hetero-Polymetallic Complexes. Molecules 29, 750, https://doi.org/10.3390/molecules29040750.

Binnemans, K., 2009. Luminescence of metallomesogens in the liquid crystal state. J. Mater. Chem. 19, 448–453, https://doi.org/10.1039/B811373D.

Bisoyi, H.K., Li, Q., 2022. Liquid Crystals: Versatile Self-Organized Smart Soft Materials. Chem. Rev. 122(5), 4887–4926, https://doi.org/10.1021/acs.chemrev.1c00761.

Blanco, H., Iguarbe, V., Barberá, J., Serrano, J. L., Elduque, A., Giménez, R., 2016. Supramolecular Columnar Liquid Crystals with Tapered-Shape Simple Pyrazoles Obtained by Efficient Henry/Michael Reactions. Chem.- Eur. J. 22(14), 4924–4930, https://doi.org/10.1002/chem.201504779.

Chen, L., Chen, C., Sun, Y., Lu, S., Huo, H., Tan, T., Li, A., Li, X., Ungar, G., Liu, F., Zhang, M., 2020. Luminescent Metallacycle-Cored Liquid Crystals Induced by Metal Coordination. Angew. Chem. Int. Ed. 59, 10143–10150, https://doi.org/10.1002/anie.201915055.

Chico, R., Domínguez, C., Donnio, B., Heinrich, B., Coco, S., Espinet, P., 2016. Isocyano-Triphenylene Complexes of Gold, Copper, Silver, and Platinum. Coordination Features and Mesomorphic Behavior. Cryst. Growth Des. 16, 6984−6991, https://doi.org/10.1021/acs.cgd.6b01206.

Cretu, C., Popa, E., Di Maio, G., Candreva, A., Buta, I., Visan, A., La Deda, M., Donnio, B., Szerb, E.I., 2023. Bimetallic liquid crystal blends based on structurally related 3d-metal coordination complexes. Chem. Commun. 59, 10616, https://doi.org/10.1039/D3CC02930A.

Cuerva, C., Cano, M., Lodeiro, C., 2021. Advanced Functional Luminescent Metallomesogens: The Key Role of the Metal Center. Chem. Rev. 121, 12966, https://doi.org/10.1021/acs.chemrev.1c00011.

Fujisawa, K., Saotome, M., Ishikawa, Y., Young, D.J., 2021. The influence of aryl substituents on the supramolecular structures and photoluminescence of cyclic trinuclear pyrazolato copper(I) complexes. Nanomaterials 11(11), 1-13, https://doi.org/10.3390/nano11113101.

Geng, H., Luo, K., Cheng, H., Zhang, S., Ni, H., Wang, H., Yu, W., Li, Q., 2017. Novel columnar metallomesogens based on cationic platinum(II) complexes without long peripheral chains. RSC Adv. 7(9) 11389, https://doi.org/10.1039/C6RA28767K.

Giménez, R., Lydon, D.P., Serrano, J.L., 2002. Metallomesogens: a promise or a fact?. Curr. Opin. Solid State Mater. Sci. 6(6), 527-535, https://doi.org/10.1016/S1359-0286(03)00009-3.

Giménez, R., Crespo, O., Diosdado, B., Elduque, A., 2020. Liquid crystalline copper(I) complexes with bright room temperature phosphorescence. J. Mater. Chem. C 8, 6552, https://doi.org/10.1039/D0TC00642D.

Hakemi, H., 2022. Metallomesogen Mixtures as Potential Materials for Application in Liquid Crystal Devices. J. Mate. Poly. Sci. 2(4), 1-5, https://doi.org/10.47485/2832-9384.1020.

Huitorel, B., Benito, Q., Fargues, A., Garcia, A., Gacoin, T., Boilot, J.-P., Perruchas, S., Camerel, F., 2016. Mechanochromic Luminescence and Liquid Crystallinity of Molecular Copper Clusters. Chem. Mater. 28, 8190–8200, https://doi.org/10.1021/acs.chemmater.6b03002

Ibrayev, N., Seliverstova, E., Valiev, R., Aymagambetova, A., Sundholm, D., 2024. The effect of heavy atoms on the deactivation of electronic excited states of dye molecules near the surface of metal nanoparticles. Phys. Chem. Chem. Phys. 26, 25986, https://doi.org/10.1039/D4CP02621G.

Ionescu, A., Godbert, N., Crispini, A., Termine, R., Golemme, A., Ghedini, M., 2012. Photoconductive Nile red cyclopalladated

metallomesogens. J. Mater. Chem. 22(44), 23617-23626, https://doi.org/10.1039/C2JM34946A.
Kadkin, O.N., An, J., Han, H., Galyametdinov, Y.G., 2008. A Novel Series of Heteropolynuclear Metallomesogens: Organopalladium Complexes with Ferrocenophane-Containing Ligands. Eur. J. Inorg. Chem. 1682–1688, https://doi.org/10.1002/ejic.200700750.
Krikorian, M., Liu, S., Swager, T.M., 2014. Columnar Liquid Crystallinity and Mechanochromism in Cationic Platinum(II) Complexes. J. Am. Chem. Soc. 136(8), 2952–2955, https://doi.org/10.1021/ja4114352.
Kumar, A., Singh, G., 2023. Recent advances and future perspectives of photoluminescent liquid crystals and their nanocomposites for emissive displays and other tunable photonic devices. J. Mol. Liq. 386, 122607, https://doi.org/10.1016/j.molliq.2023.122607.
Micutz, M., Iliş, M., Staicu, T., Dumitraşcu, F., Pasuk, I., Molard, Y., Roisnel, T., Cîrcu, V., 2014. Luminescent liquid crystalline materials based on palladium(II) imine derivatives containing the 2-phenylpyridine core. Dalton Trans. 43, 1151, https://doi.org/10.1039/C3DT52137K.
Pastor, M.J., Cuerva, C., Fernandez-Lodeiro, A., Lodeiro, C., Campo, J.A., Cano, M., 2018. Designing Zn(II) complexes as a support of bifunctional liquid crystal and luminescent materials. Dyes Pigments 149, 37-50, https://doi.org/10.1016/j.dyepig.2017.09.039.
Popa, E., Andelescu, A.A., Ilies, S., Visan, A., Cretu, C., Scarpelli, F., Crispini, A., Manea, F., Szerb, E.I., 2023. Hetero-Bimetallic Ferrocene-Containing Zinc(II)-Terpyridyl-Based Metallomesogen: Structural and Electrochemical Characterization. Materials 16, 1946, https://doi.org/10.3390/ma16051946.
Santoro, A., Whitwood, A.C., Gareth Williams, J.A., Kozhevnikov, V.N., Bruce, D.W., 2009. Synthesis, Mesomorphism, and Luminescent Properties of Calamitic 2-Phenylpyridines and Their Complexes with Platinum(II), Chem. Mater. 21, 3871–3882, https://doi.org/10.1021/cm9012156.
Soria, L., Cano, M., Campo, J.A., Rosario Torres, M., Lodeiro, C., 2016. Silver compounds based on N,N,N-tridentate pyridylpyrazolate ligands. An opportunity to build cyclic trimetallic and oligomeric luminescent liquid crystals. Polyhedron 125, 141-150, http://dx.doi.org/10.1016/j.poly.2016.10.049.
Szerb, E.I., Crispini, A., Aiello, I., La Deda, M., 2022. Springer Handbook of Inorganic Photochemistry; Part XII: Inorganic Materials for Optoelectronics, 62: Liquid Crystals, Section editor: Eli Zysman-Colman; Bahnemann, D.W., Patrocinio, A.O.T., Eds.; Springer Nature: Cham, Switzerland, pp. 1811–1848.
Titov, A.A., Filippov, O.A., Smol'yakov, A.F., Godovikov, I.A., Shakirova, J.R., Tunik, S.P., Podkorytov, I.S., Shubin, E.S., 2019. Luminescent Complexes of the Trinuclear Silver(I) and Copper(I) Pyrazolates Supported with Bis(diphenylphosphino)methane. Inorg. Chem. 58, 8645−8656, https://doi.org/10.1021/acs.inorgchem.9b00991
Wang, Y., Fan, J., Shi, J., Qi, H., Baranoff, E., Xie, G., Li, Q., Tan, H., Liu, Y., Zhu, W., 2016. Influence of integrated alkyl-chain length on the mesogenic and photophysical properties of platinum-based metallomesogens and their application for polarized white OLEDs. Dyes Pigments 133, 238-247, https://doi.org/10.1016/j.dyepig.2016.05.024.
Wang, Y., Chen, Q., Li, Y., Liu, Y., Tan, H., Yu, J., Zhu, M., Wu, H., Zhu, W., Cao, Y., 2012. Highly Dichroic Metallomesogen of Dinuclear Platinum Complex: Synthesis and Liquid Crystal and Photophysical Properties. J. Phys. Chem. C 116, 5908–5914, https://doi.org/10.1021/jp211976x.
Wenzel, M., Bigaeva, E., Richard, P., Le Gendre, P., Picquet, M., Casini, A., Bodio, E., 2014. New heteronuclear gold(I)–platinum(II) complexes with cytotoxic properties: Are two metals better than one? J. Inorg. Biochem. 141, 10–16, https://doi.org/10.1016/j.jinorgbio.2014.07.011
Wu, X., Xie, G., Cabry, C.P., Xu, X., Cowling, S.J., Bruce, D.W., Zhu, W., Baranoff, E., Wang, Y., 2018. Linearly Polarized Electroluminescence from Ionic Iridium Complex-based Metallomesogens: The Effect of Aliphatic-Chain on Their Photophysical Properties. J. Mater. Chem. C 6, 3298–3309, https://doi.org/10.1039/C7TC05421A.

Su, P.Y.S., Hsu, S.J., Tseng, J.C.W., Hsu, H.-F., Wang, W.-J., Lin, I.J.B., 2016. Polynuclear Silver(I) Triazole Complexes: Ion Conduction and Nanowire Formation in the Mesophase. Chem. Eur. J. 22(1), 323-330, https://doi.org/10.1002/chem.201502823.

ISSN 1582-1021
e-ISSN 2668-4764
Edited by "Aurel Vlaicu" University of Arad Publishing House, Arad, Romania

10.62591/Scien.Tech.Bull-Chem.FoodSci.Eng.2024.21.05

Article

SYNTHESIS, STRUCTURAL AND PHOTOPHYSICAL PROPERTIES OF A NEW DITOPIC TERPYRIDINE-BASED PROLIGAND BEARING DISELENIDE UNITS

Adelina A. ANDELESCU[1*], Evelyn POPA[1], Elisabeta-Ildyko SZERB[1]

[1] *"Coriolan Drăgulescu" Institute of Chemistry, Romanian Academy, 24 Mihai Viteazu Blvd., 300223 Timisoara, Romania*

Abstract: *The present paper describes the synthesis and characterization of a new ditopic proligand with two terpiridines linked by a diselenide unit, obtained by a Steglich esterification procedure between a biscarboxylic acid functionalized with a diselenide unit and 4-([2,2':6',2''-terpyridin]-4'-yl)phenol. The compound was characterized by FT-IR, NMR (1D and 2D) and UV-Vis spectroscopies and ESI-MS analysis. Moreover, the photophysical properties of the ditopic ligand were investigated in freshly prepared dichloromethane solution. The compound was found to be emissive with a maximum centered at 354 nm.*

Keywords: heterocycles; N-donor ligand; ditopic ligand; oligopyridines;

INTRODUCTION

The molecule 2,2':6',2''-terpyridine (*tpy*) is a tridentate ligand with three nitrogen coordination sites (Mughal et al. 2020) and was first reported in 1932 by Morgan and Burstall as one of 20 products of the reaction when they heated pyridine and anhydrous iron(III) chloride in an autoclave (Morgan and Burstall 1932).

Since then, *tpy* and its derivatives have received attention due to their ability to easily form metal complexes with main-group, *d*-block and lanthanide elements (Fallahpour 2002, Mughal et al. 2020). *Tpy* derivatives and their metal complexes have been studied in supramolecular chemistry and catalysis (Wey et al. 2019), electrochemical sensors (Negrea et al. 2022, Popa et al. 2023), as DNA binders and medicinal chemistry (Abhijnakrishna et al. 2023), etc.

Various synthetic procedures have been employed for the synthesis of *tpy* scaffolds (Fallahpour 2002, Kainat el al. 2024), such as cross-coupling [Li et al. 2011, Robo et al. 2014, Zibaseresht 2019] or ring assembly methods (Fernandes et al. 2018, Wang et al. 2019).

Among them, the one-pot Kröhnke reaction [Kröhnke 1976] is the most commonly employed method, and it involves the reaction of two equivalents of a substituted acetylpyridine derivative with an aldehyde in a basic medium and in the presence of an ammonia source. Following the Kröhnke methodology, a wide variety of 4'-substituted *tpy* derivatives were reported (Kainat et al. 2024).

Ditopic ligands, with two different, separated metal-binding domains in their structures, can form two types of coordination compounds: homo and hetero multi-metallic complexes (Salimova et al. 2020, Schäfer et al. 2021)

The first of these are complexes in which both ligand fragments, coordinate the same metal ion. Polymetallic complexes may be obtained using ditopic terpyridinyl units resulting in luminescent materials or electrochemical sensors [Indelli et al. 1998, Andelescu et al. 2024].

Moreover, the synthesis of ditopic *tpy* derivatives with an additional donor atom (such as: sulphur or selenium) is of interest due to their ability to bind nanoparticles (Yee et al. 2003, Rudakovskaya et al. 2010, Romashkina et al. 2013, Margandan et al. 2017, Popa *et al.* 2024).

On this background, we report the synthesis and characterization of a new ditopic *tpy* proligand, namely bis(4-([2,2':6',2''-terpyridin]-4'-yl)phenyl)6,6'-diselanediyldihexanoate (Figure 1), which contains additionally an aromatic ring on its structure, compared to the one previously reported by our group (Popa *et al.* 2024). Also, the insertion of selenium atom into the structure may lead to compounds with potential applications as drugs (Banerjee et al. 2017). Due

to the presence of three nitrogen rings, the ditopic terpyridine-based ligand may find future applications as coordination polymers (Shu *et al.* 2022), whereas the presence of a diselenide unit enables them to be studied as drug delivery systems or anticancer drugs (Han et al. 2019).
The compound was structurally characterized by FT-IR, NMR, and UV-Vis spectroscopies. The proposed structure is supported by the ESI-MS analysis. The photophysical properties of the final compound were investigated in freshly prepared dichloromethane solution.

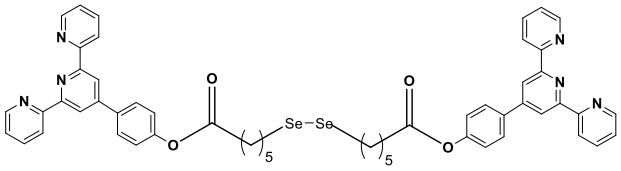

Compund 3

Figure 1. Proposed chemical structure of the terpyridine derivative.

MATERIALS AND METHODS

N,N′-dicyclohexylcarbodiimide (DCC), 4-dimethylaminopyridine (4-DMAP), 2-acetylpyridine, 4-methoxybenzaldehyde, anhydrous THF, and DMF were purchased from Sigma Aldrich and used without any further purification. The solvents used for the column chromatography were purchased from Carlo Erba. Neutral Al_2O_3 60 and spectrofluorimetric grade dichloromethane were purchased from VWR.
Melting point was determined by optical microscopy using an Olympus BX53M polarizing microscope (POM) equipped with a Linkam hot-stage.
Infrared spectra (KBr pellets) in the range 4000-400 cm^{-1} range were recorded on a Cary 630 FT-IR spectrophotometer.
The ^{1}H-NMR spectra were recorded either on a Bruker Fourier 300 MHz spectrometer or Bruker Avance 300) in $CDCl_3$ or DMSO-d_6. 1D and 2D NMR experiments were recorded on Bruker Avance III HD – 500 MHz spectrometer in $CDCl_3$.
Spectrofluorimetric grade dichloromethane was used for the photophysical investigations in solution. The absorption spectrum in solution was recorded on an Agilent Cary 60 spectrophotometer using quartz cuvettes of 1 cm path length. The emission spectrum were recorded on Horiba Fluoromax Plus spectrofluorometer. The luminescence quantum yields of the samples in the solution were recorded using a QuantaPhi-2 integrating sphere with 121 mm internal diameter with reflectivity from 250 to 2500 nm.
High-resolution mass spectral (HRMS) spectra was recorded on Orbitrap IQ-X Mass Spectrometer from Thermo Scientific using an electrospray ionization (ESI) technique. The equipment was operated in positive-ion mode and ion transfer parameters were optimized to enable detection of ions in a m/z range between 150 and 2000. The employed parameters are listed in Table 1. The system was externally calibrated by using Pierce FlexMix Calibration Solution from Thermo Scientific. The data was collected in positive MS scan mode and processed using Thermo Scientific Xcalibur 4.7 software.

Table 1. Employed parameters for ESI-MS technique

Source parameters	**Values**
Ionization mode	Positive electrospray ionization
Spray voltage	3200 V
Sheath gas flow rate	5 Arb
Auxiliary gas flow rate	2 Arb
Sweep gas flow rate	0 Arb
Ion transfer tube temperature	300℃
Vaporizer temperature	20℃
Acquisition parameters	**Values**
Detector type	Orbitrap
Orbitrap resolution	120000
Scan range	400-1500 m/z
AGC target	100%
Injection time	100 ms
Syringe flow	5 µl/min

EXPERIMENTAL SECTION

*Synthesis of 4-([2,2':6',2''-terpyridin]-4'-yl)phenol, **2***

Compound **2** was obtained in two steps following a reported procedure (Bahrami *et al.* 2017) and the results agree well with the reported data.
I1: white solid (0.91 g, 2.68 mmol, 65.6 %).
FT-IR (KBr, cm^{-1}): 2992 (νC-H); 1600 – 1431 (ν (C=N)) and (ν (C=C)).
^{1}H-NMR (300 MHz, $CDCl_3$, δ/ppm): 8.75 - 8.59 (m, 6H), 7.94-7.68 (m, 4H), 7.42-7.25 (m, 2H), 7.12-6.92 (m, 2H), 3.89 (s, 3H);

Compound **2**: pale grey solid (0.720 g, 2.21 mmol, 93 %).

FT-IR (KBr, cm^{-1}): 3250 (νOH, broad); 1616 – 1430 (ν (C=N)) and (ν (C=C)).

^{1}H-NMR (300 MHz, DMSO-d6, δ/ppm): 8.77-8.70 (d, 2H), 8.69-8.55(d, 4H), 8.07- 7.95 (td, 2H), 7.81 -7.60(m, 2H), 7.57- 7.43 (m, 2H), 7.00- 6.95(dd, 2H).

*Synthesis of bis(4-([2,2':6',2''-terpyridin]-4'-yl)phenyl) 6,6'-diselanediyldihexanoate, **3***

0.09 g (0.23 mmol) of compound **1**, 0.166 g (0.51 mmol) of compound **2** and 22.65 mg (0.1854 mmol) of 4-DMAP in 10 mL THF and 1 mL of DMF were stirred at room temperature under argon atmosphere for 30 minutes, then 0.105 g (0.51 mmol) of DCC in 3 mL of THF were added dropwise. The consumption of the starting materials was monitored on TLC (Al_2O_3: $CHCl_3$:hexane = 1:1). After 5 days, the reaction mixture was taken to dryness, dissolved in $CHCl_3$, washed with distilled water (3x50 mL), the organic phase was dried over anhydrous sodium sulfate, filtered and taken to dryness. The residue was taken with AcOEt and the undissolved precipitate was filtered (to remove the DCU biproduct) and mother liquor was taken to dryness. This procedure was repeated 3 times. The pure compound was isolated after purification on column chromatography using Al_2O_3 as stationary phase in $CHCl_3$:hexane = 1:1, resulting in a yellow gel (0.058 mmol, 25%).

Melting point: 83-85ºC.

FT-IR (KBr, cm^{-1}): 1762 (νC=O); 1605 – 1412 (ν (C=N)) and (ν (C=C)).

^{1}H-NMR (500 MHz, $CDCl_3$, δ/ppm): 8.67 – 8.62 (m, 4H), 8.58 (dt, *J* = 7.9, 1.1 Hz, 2H), 7.86 – 7.82 (m, 2H), 7.80 (td, *J* = 7.7, 1.8 Hz, 2H), 7.27 (ddd, *J* = 7.5, 4.8, 1.3 Hz, 2H), 7.18 – 7.15 (m, 2H), 2.90 (t, *J* = 7.4 Hz, 2H), 2.55 (t, *J* = 7.4 Hz, 2H), 1.81 – 1.71 (m, 4H), 1.50 (tdd, *J* = 9.9, 8.6, 5.1 Hz, 2H).

^{13}C-NMR (126 MHz, $CDCl_3$, δ/ppm) δ 171.88, 156.07, 155.88, 151.49, 149.38, 149.06, 136.99, 136.02, 128.46, 123.90, 122.11, 121.43, 118.83, 34.27, 30.60, 29.68, 28.92, 24.41.

HR-MS ($C_{54}H_{48}N_6O4Se_2$+H): simulated: 1005.21442, found: 1005.21402

RESULTS AND DISCUSSIONS

The preparation of compound **3,** required the synthesis of the starting materials: 6,6'-(1,2-diselanediyl)dihexanoic acid, **1** and 4-([2,2':6',2"-terpyridin]-4'-yl)phenol, **2.**

6,6'-(1,2-diselanediyl)dihexanoic acid, **1** was obtained and fully characterized in a previously published paper of our group [Popa *et al.* 2024].

For the synthesis of 4-([2,2':6',2"-terpyridin]-4'-yl)phenol, **2** a reported procedure was followed, which involved a one-pot Kröhnke condensation between 4-methoxybenzaldehyde and 2-acetylpyridine, in a basic media [Bahrami *et al.* 2017]. The pure compound was isolated after a recrystallization from methanol [Chen et al. 2018]. The intermediate **I1** was then demethylated under strong acidic conditions to yield the desired compound **2**. The reaction pathway is presented in Scheme 1.

The desired compound **3**, bis(4-([2,2':6',2"-terpyridin]-4'-yl)phenyl) 6,6'-diselanediyldihexanoate was obtained adapting a procedure reported by our group (Scheme 1, Popa *et al.* 2024), through a Steglich esterification reaction between compound **1** and **2** equivalents of compound **2**, using DCC as a coupling reagent in the presence of 4-DMAP as catalyst.

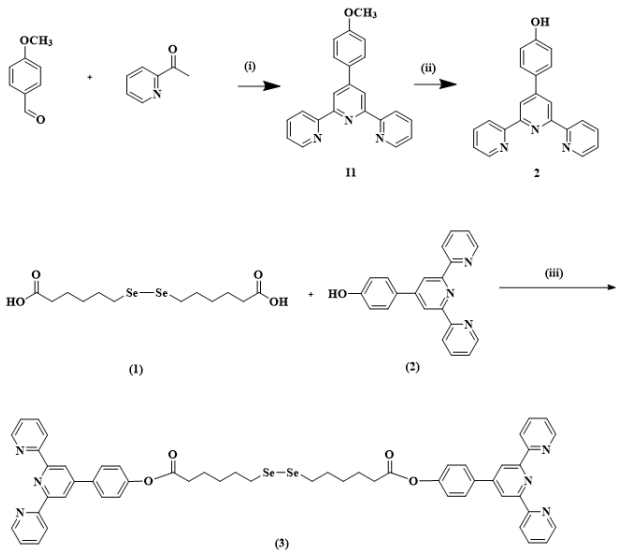

Scheme 1. Reaction pathway for the synthesis of compounds **2** and **3**. Reagents and conditions: (i) KOH, EtOH, NH_4OH, ΔT, 24 hours; (iii) DCC, 4-DMAP, THF-DMF (10-1 V/V), inert atmosphere, r.t, 5 days;

Compound **3** was isolated as a yellow waxy solid. Its structure was proposed based on spectroscopic methods: FT-IR, NMR (1D and 2D) spectroscopy and MS spectrometry.

The first confirmation of the formation of the desired compound **3**, was gained from FT-IR analysis through the shift of the characteristic absorption band of the carbonyl group ($\nu_{C=O}$) from 1694 cm^{-1} in compound **1**, to 1762 cm^{-1} in compound **3,** which is characteristic of the C=O bond in esters. Moreover, the stretching vibration of the ν_{C-Se} bond is identified at 635 cm^{-1} in compound **1**, and 640 cm^{-1} in compound **3** (Helios et al. 2015). The main characteristic absorption bands of the compound are reported in Table 2.

Table 2. Assignment of the characteristic absorption bands of the starting materials and the final compound **3**.

Cpd	Assignment of the characteristic absorption bands (wavenumber values in cm^{-1})		
	$\nu_{(C=O)}$	$\nu_{(C=N \text{ and } C=C)}$	$\nu_{(C-Se)}$
1*	1694	-	635
2	-	1616 – 1430	-
3	1762	1605 – 1412	641
* Data reported in Popa *et al.* 2024			

In order to confirm the proposed structure, 1D and 2D NMR spectra were recorded on a Bruker 500 MHz instrument. This allowed us to fully index all the protons and carbon atoms based on ^{1}H-^{1}H COSY (Correlation Spectroscopy), HSQC (Heteronuclear Single Quantum Coherence), and HMBC (Heteronuclear Multiple Bond Correlation) experiments. The results are summarized in Table 3.

Table 3. 1D and 2D NMR data of compound 3 recorded in $CDCl_3$

Atom label	**^{1}H**	**^{13}C**	**COSY**	**HMBC**
C	1.50 (tdd, *J* = 9.9, 8.6, 5.1 Hz, 2H)	28.92	B,D	A, D, E
B, D	1.81 – 1.68, m, 4H	30.60 (B), 24.41 (D)	A,E,C	A, D, E, F,
E	2.55, t, *J* = 7.4 Hz, 2H	34.27	D	D,C,F
A	2.90 (t, J = 7.4 Hz, 2H),	29.68	B	-
F	-	171.88	-	-
1*	8.67 – 8.62 (m, 4H)	149.06	2	2, 3
2	7.27 (ddd, J = m, 2H)	123.90	1, 3	1, 4, 5, 6
3	7.80 (td, *J* = 7.7, 1.8 Hz, 2H)	136.99	1, 2	1, 4, 6
4	8.58 (dt, J = 7.9, 1.1 Hz, 2H)	121.43	3	2, 5, 6
5	-	155.88	-	-
6	-	156.07	-	-
7*	8.67 – 8.62 (m, 4H)	118.83	-	4, 5, 6, 9, 11,
8	-	149.38	-	-
9	-	136.02	-	-
10	7.86 – 7.82 (m, 2H)	128.46	11	8, 11, 12
11	7.23 – 7.08 (m, 2H)	122.11	10	9, 12
12	-	151.49	-	-
* Peaks appear overlapped in ^{1}H-NMR spectra in total 4H				

The ^{1}H-NMR spectrum (Figure 2) presented all the expected signals of the protons, and their integration agrees with the proposed structure, while the ^{13}C-NMR spectra contained all the expected signals for the 18 carbon atoms from half of the molecule.

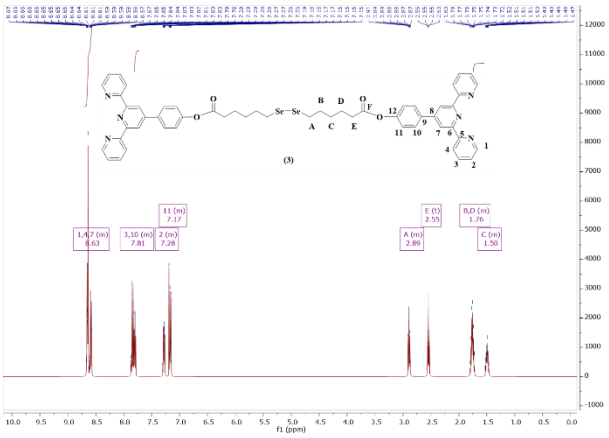

Figure 2. The ^{1}H-NMR spectrum of compound **3** recorded in $CDCl_3$ and the atom labeling.

Finally, the proposed structure is supported by the ESI-MS analysis (Figure 3).

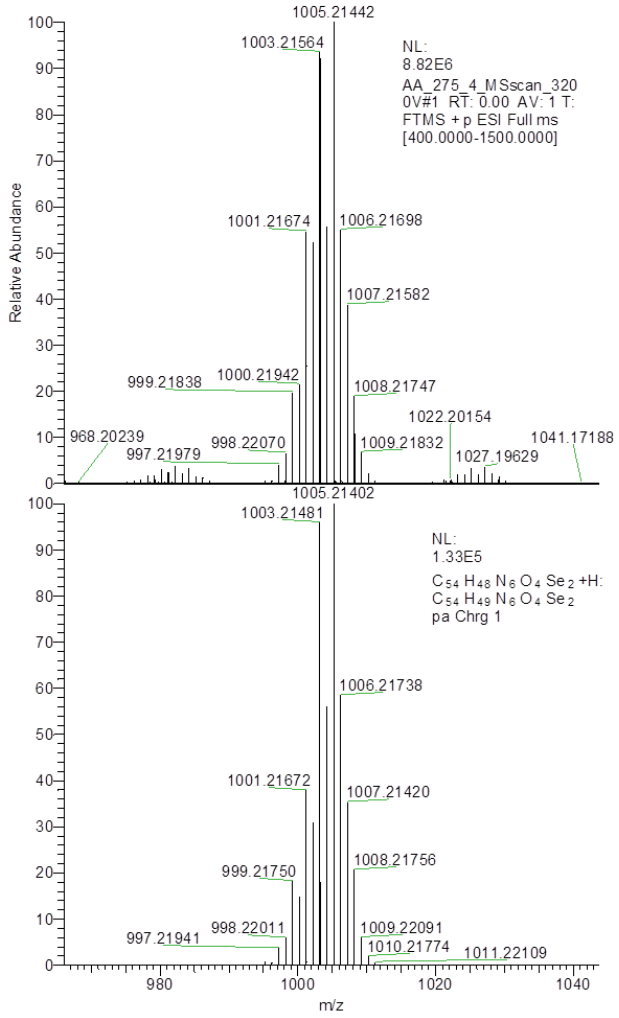

Figure 3. Simulation vs. experimental MS spectra for compound **3**.

The photophysical properties of compound **3** (absorption, emission maxima and lifetimes of the excited states) were determined in freshly prepared dichloromethane solution and the data are presented in Figure 4 and summarized in Table 4. From the absorption spectra several information could be obtained: the absorptions band from 252 and 280 nm are due to π-π* from the *tpy* ring (Toledo et al. 2015), whereas the shoulder centered at 311 nm may be due to the diselenide bond (Back et al. 1983). It is well known that the *tpy* scaffolds present fluorescence properties at room temperature (Costa et al. 2015), therefore the emission spectrum was recorded after excitation at 311 nm, presenting an emission band centered 354 nm.

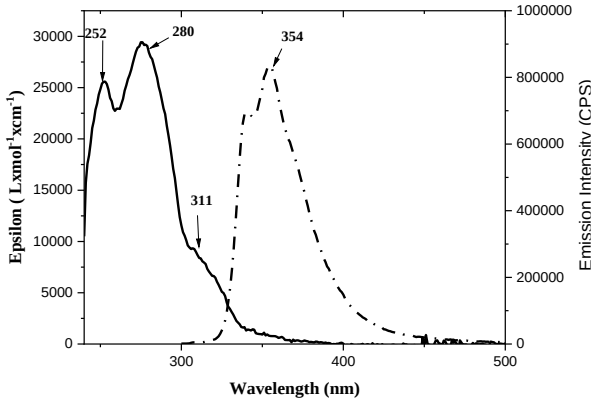

Figure 4. Absorption (solid line) and emission (dashed line) of compound **3** in CH_2Cl_2 solution (c= 5*10^{-6} mol/L).

Table 4. Photophysical properties of compound **3** in solution (c= 5*10^{-6} mol/L).

Sample	**Abs, λ_{max}/nm (ε/M^{-1} cm^{-1})**	**Em, λ_{max}/nm**	**ϕ /%**
1*	308 (640)	-	-
2**	286, 330-410	384	-
3	252 (25512) 280 (29364) 311 (9077)	354 (λ_{ex}=311 nm)	6.33

* Data reported by Popa *et al.* 2024
** Data recorded in ethanol solution reported by Sierra *et al.* 2018

Structurally similar terpyridine ligands with disulfide moieties were reported by Majouga *et. al* 2010, but their photophysical properties were not investigated, whereas in case of those with diselenide units, there is only one reported by our group (Popa *et al.* 2024) with its emission maxima centered at 349 nm. Compared to the compound reported in the present paper it presents a small bathochromic shift of 5 nm. The compound presented a quantum yield value of 6.33 %.

Recently it was mentioned that linear diselenides quenched fluorescence through a synergistic combination of intramolecular charge transfer, ICT and Förster resonance energy transfer, FRET (Ma et al. 2024). Therefore, the low quantum yield value may be attributed to the quenching effect of the diselenide moiety.

CONCLUSIONS

A new terpyridine derivative containing a diselenide unit was obtained and its structure was confirmed based on FT-IR, NMR (1D and

2D) investigations and HR-MS spectrometry. Its optical properties were investigated in freshly prepared dichloromethane solutions by UV-Vis and fluorescence measurements.

ACKNOWLEDGEMENTS

This work was supported by a grant of the Ministry of Research, Innovation and Digitization, CNCS/CCCDI – UEFISCDI, project number PN-III-P1-1.1-PD-2021-0427, within PNCDI III.
Authors acknowledge the Romanian Academy, Program 4 and the infrastructure support granted by the project RO-OPENSCREEN, MySMIS code: 127952, Contract no. 371/20.07.2020, co-financed by European Regional Development Fund through the Competitiveness Operational Program 2014-2020.

REFERENCES

Andelescu, A.A, Candreva, A., Popa, E., Visan, A., Cretu, C., La Deda, M., Szerb, E.I., 2024. Role of the Environment Polarity on the Photophysical Properties of Mesogenic Hetero-Polymetallic Complexes. Molecules 29, 750. https://doi.org/10.3390/molecules29040750

Abhijnakrishna, R., Magesh, K., Ayushi, A., Velmathi, S., 2023. Advances in the Biological Studies of Metal-Terpyridine Complexes: An Overview From 2012 to 2022. Coordination Chemistry Reviews 496, 215380. https://doi.org/10.1016/j.ccr.2023.215380

Bahrami, K., Khodaei, M.M., Meibodi, F.S., 2017. Suzuki and Heck cross-coupling reactions using ferromagnetic nanoparticle-supported palladium complex as an efficient and recyclable heterogeneous nanocatalyst in sodium dodecylsulfate micelles. Applied Organometallic Chemistry 31(6), e3627. https://doi.org/10.1002/aoc.3627

Back, T.G., Codding, P.W., 1983. Studies of the dihedral angle of a crowded diselenide by X-ray crystallography and ultraviolet spectroscopy. Canadian Journal of Chemistry 61, 2749–2752. https://doi.org/10.1139/v83-472

Banerjee, B., Koketsu, M., 2017. Recent developments in the synthesis of biologically relevant selenium-containing scaffolds. Coordination Chemistry Reviews 339, 104–127.

Costa, J., Ruloff, R., Burai, L., Helm, L., Merbach, A.E., 2005. Rigid MIIL2Gd2III (M ¼ Fe, Ru) complexes of a terpyridine-based heteroditopic chelate: a class of candidates for MRI Contrast agents. Journal of the American Chemical Society 1102, 5147-5157. https://doi.org/10.1021/ja0424169

Chen, F., Tian, Y.-K., Chen, Y., 2018. Controlled formation of main chain supramolecular polymer based on metal–ligand interaction and thiolene click reaction. Chemistry - An Asian Journal 13, 3169 – 3172. https://doi.org/10.1002/asia.201801235

Fernandes, S.S.M., Belsley, M., Ciarrocchi, C., Licchelli M., Raposo, M.M.M., 2019. Terpyridine derivatives functionalized with (hetero)aromatic groups and the corresponding Ru complexes: Synthesis and characterization as SHG chromophores. Dyes and Pigments 150, 49–58. https://doi.org/10.1016/j.dyepig.2017.10.046

Han, W., Zhang, S., Qian, J., Zhang, J., Wang, X., Xie, Z., Xu, B., Han, Y., Tian, W., 2019. Redox Responsive Fluorescent nanoparticles based on Diselenide-containing AIEgens for Cell imaging and Selective Cancer Therapy. Chemistry - An Asian Journal 14, 1745–1753. h**ttps://doi.org/10.1002/asia.201801527**

Helios, K., Pietraszko, A., Zierkiewicz, W., Wójtowicz, H., Michalska, D, 2015. The crystal structure, infrared, Raman and density functional studies of bis(2-aminophenyl) diselenide. Polyhedron 30, 2466–2472. https://doi.org/10.1016/j.poly.2011.06.040

Kainat, S.F., Hawsawi, M.B., Mughal, E.U., Naeem, N., Almohyawi, A.M., Altass, H.M, Hussein, E.M., Sadiq, A., Moussa, Z., Abd-El-Aziz, A.S, Ahmed, S.A., 2024. Recent developments in the synthesis and applications of terpyridine-based metal complexes: a systematic review. RSC Advances 14, 21464-21537. https://doi.org/10.1039/D4RA04119DKröhnke, F., 1976. The Specific Synthesis of Pyridines and Oligopyridines. Synthesis, 1–24.

Li, J., Sato, T., Li, H., Higuchi, M., 2011. Synthesis of Unsymmetrical, Monosubstituted Bis-terpyridine Derivatives via Suzuki-Miyaura Cross-Coupling. Synthesis 9, 1361-1364.

Ma, T., Gao, H., Wu, J., Zhao, J., Chang, B., Zhang, Z., Zhang, S., Baoxin, Z., Fang, J.,

2024. Diselenides as novel effective fluorescence quenchers to construct a two-photon fluorescent probe for thiols in a mouse stroke model. Chemical Communications 61, 1910-1913. https://doi.org/10.1039/D4CC06286H

Majouga, A.G., Romashkina, R.B., Kashaev, A.S., Rahimov, R.D, Beloglazkina, E.K., Zyk, N.V., 2010. New organic ligands of the terpyridine series: modification of gold nanoparticles, preparation of coordination compounds with Cu(I), catalysis of oxidation reactions. Chemistry of Heterocyclic Compounds 46, 1076–1083. https://doi.org/10.1007/s10593-010-0630-y

Margandan, K., Jebastin, S.J.M, 2017. Synthesis And Characterization Of Bismercapto (2, 2′:6′, 2″-Terpyridine) Ru(II)-Complexes Stabilized Gold Nanoparticles And Their Electro Catalytic Reduction Of Nitrite. Journal of the Chilean Chemical Society 62(4), 3691-3699.

Morgan, G.T., Burstall, F.H., 1932. Dehydrogenation of pyridine by anhydrous ferric chloride. Journal of the Chemical Society, Abstracts, 20-30. https://doi.org/10.1039/JR9320000020

Mughal, E.U., Mirzaei, M., Sadiq, A., Fatima, S., Naseem, A., Naeem, N., Fatima, N., Kausar, S., Altaf, A.A., Muhammad, Z.N., Ahmad, K.B., 2020. Terpyridine-metal complexes: effects of different substituents on their physico-chemical properties and density functional theory studies. Royal Society Open Science 7 (11), 201208. https://doi.org/10.1098/rsos.201208

Negrea, S., Andelescu, A.A., Ilies, S., Cretu, C., Cseh, L., Rastei, M., Donnio, B., Szerb, E.I., Manea, F., 2022. Design of Nanostructured Hybrid Electrodes Based on a Liquid Crystalline Zn(II) Coordination Complex-Carbon Nanotubes Composition for the Specific Electrochemical Sensing of Uric Acid. Nanomaterials 12(23), 4215. https://doi.org/10.3390/nano12234215

Popa, E., Andelescu, A.A., Ilies (b. Motoc), S., Visan, A., Cretu, C., Scarpelli, F., Crispini, A., Manea, F., Szerb, E.I., 2023. Hetero-Bimetallic Ferrocene-Containing Zinc(II)-Terpyridyl-Based Metallomesogen: Structural and Electrochemical Characterization. Materials 16(5), 1946. https://doi.org/10.3390/ma16051946

Popa, E., Andelescu, A.A., Badea, V., Svera, P., Szerb, E.I., 2024. Bis(2,6-di(pyridin-2-yl)pyridin-4-yl)-6,6′-(1,2-diselanediyl)dihexanoate. Molbank 2024(1), M1752. https://doi.org/10.3390/M1752

Robo, M.T., Prinsell, M.R., Weix, D. J., 2014. 4,4′,4″-Trimethyl-2,2′:6′,2″-terpyridine by Oxidative Coupling of 4-Picoline. The Journal of Organic Chemistry 79 (21), 10624–10628. https://doi.org/10.1021/jo501925s

Rudakovskaya, P.G., Beloglazkina, E.K., Majouga, A.G., Zyk, N.V., 2010. Synthesis and characterization of terpyridine-type ligand-protected gold-coated Fe3O4 nanoparticles. Mendeleev Communications 20, 158–160. https://doi.org/10.1016/j.mencom.2010.05.012

Romashkina, R.B., Majouga, A.G., Beloglazkina, E.K., Pichugina D.A., Askerka, M.S., Moiseeva, A.A., Rakhimov, R.D., Zyk, N.V., 2013. Sulfur-containing terpyridine derivatives: synthesis, coordination properties, and adsorption on the gold surface. Russian Chemical Bulletin 61, 2265–2281. https://doi.org/10.1007/s11172-012-0322-0

Salimova, I.A., Berezina, A.V., Barskaya, E.S., Abramovich, M.S. , Lyssenko K.A., Zyk, N.V., Beloglazkina, E.K., 2020. Syntheses of terpyridine-pyridylbenzothiazole linked ditopic ligands and their copper(II) complexes. Polyhedron 179, 114403. https://doi.org/10.1021/ic900932j

Schäfer, B., Suryadevara, N., Greisch, J.-F., Fuhr, O., Kappes, M.M., Ruben, M., 2021. Ditopic Hexadentate Ligands with a Central Dihydrobenzo-diimidazole Unit Forming a [2x2] Zn_4 Grid Complex. European Journal of Organic Chemistry 2021(16), 2301-2310. https://doi.org/10.1002/ejoc.202100230

Sierra, C., Castro Agudelo, B., Ochoa-Puentes, C., Rodriguez-Cordoba, W.Y., Reiber, A., 2018. Synthesis, characterization, X-ray crystal structure and DFT calculations of 4-([2,2':6',2''-terpyridin]- 4'-yl)phenol. Revista Colombiana de Química. 47, 1.

Shu, M., Tao, J., Han, Y., Fu, W., Li X., Zhang, R., Liu, J., 2022. Molecular engineering of terpyridine-Fe(II) coordination polymers consisting of quinoxaline-based π-spacers toward enhanced electrochromic performance. Polymer 256, 125231. https://doi.org/10.1016/j.polymer.2022.125231

Toledo, D., Baggio, R., Freire, E., Vega, A., Pizarro, N., Moreno, Y., 2015. Structure and spectroscopy of two new bases for building block: Terpyridine derivatives. Journal of Molecular Structure 1102, 18-24. https://doi.org/10.1016/j.molstruc.2015.08.030

Wang, H., Li, Y., Yu, H., Song, B., Lu, S., Hao, X.-Q., Zhang, Y., Wang, M., Hla, S.-W., Li, X., 2019. Combining synthesis and self-assembly in one pot to construct complex 2D Metallo-Supramolecules Using Terpyridine and Pyrylium Salts. Journal of the American Chemical Society 141(33), 13187–13195. https://doi.org/10.1021/jacs.9b05682

We,i C., He, Y., Shi, X., Song, Z., 2019. Terpyridine-metal complexes: Applications in catalysis and supramolecular chemistry. Coordination Chemistry Reviews 385, 1-19. https://doi.org/10.1016/j.ccr.2019.01.005

Yee, C.K., Ulman, A., Ruiz, J.D., Parikh, A., White, H., Rafailovich, M., 2003. Alkyl Selenide- and Alkyl Thiolate-Functionalized Gold Nanoparticles: Chain Packing and Bond Nature. Langmuir 19, 9450-9458. https://doi.org/10.1021/la020628i

Zibaseresht, R., 2019. Synthesis and characterization of a new ditopic bipyridine-terpyridine bridging ligand using a Suzuki cross-coupling reaction. Arkivoc 2019, part vi. https://doi.org/10.24820/ark.5550190.p011.044

ISSN 1582-1021
e-ISSN 2668-4764
Edited by "Aurel Vlaicu" University of Arad Publishing House, Arad, Romania

10.62591/Scien.Tech.Bull-Chem.FoodSci.Eng.2024.21.06

Published by "AUREL VLAICU" University of Arad Publishing House, Arad, Romania, 2024